

Are atoms spherical?

Tomoya Naito^{1, 2}, Shimpei Endo^{3, 4}, Kouichi Hagino⁵, and Yusuke Tanimura^{3, 6}

¹ *Department of Physics, Graduate School of Science, The University of Tokyo, Tokyo 113-0033, Japan*

² *RIKEN Nishina Center, Wako 351-0198, Japan*

**E-mail: tomoya.naito@riken.jp*

³ *Department of Physics, Tohoku University, Sendai 980-8578, Japan*

⁴ *Frontier Research Institute for Interdisciplinary Science, Tohoku University, Sendai 980-8578, Japan*

**E-mail: shimpei.endo@nucl.phys.tohoku.ac.jp*

⁵ *Department of Physics, Kyoto University, Kyoto 606-8502, Japan*

**E-mail: hagino.kouichi.5m@kyoto-u.ac.jp*

⁶ *Graduate Program on Physics for the Universe, Tohoku University, Sendai 980-8578, Japan*

**E-mail: tanimura@nucl.phys.tohoku.ac.jp*

.....
Atomic nuclei can be spontaneously deformed into non-spherical shapes as many-nucleon systems. We discuss to what extent a similar deformation takes place in many-electron systems. To this end, we employ several many-body methods, such as the unrestricted Hartree-Fock method, post-Hartree-Fock methods, and the density functional theory, to compute the electron distribution in atoms. We show that the electron distribution of open-shell atoms is deformed due solely to the single-particle valence orbitals, while the core part remains spherical. This is in contrast to atomic nuclei, which can be deformed collectively. We qualitatively discuss the origin for this apparent difference between atoms and nuclei by estimating the energy change due to deformation. We find that nature of the interaction plays an essential role for the collective deformation.
.....

Subject Index A63, D10, D12, J33

1. Introduction

Atoms and atomic nuclei share common features as quantum many-body systems of interacting fermions [1]. In atoms, the inter-particle interaction is the repulsive Coulomb interaction between electrons, and there exists the spherical external Coulomb potential due to the nucleus. On the other hand, in atomic nuclei, the inter-particle interaction is the attractive nuclear force between two or more nucleons, with no external potential. Despite the differences in the fundamental interactions, many similar properties have been observed in both systems, such as the shell structure and the associated magic numbers [2, 3].

One of the most important properties of atomic nuclei is the collective nuclear deformation, which is evidenced by the characteristic rotational spectra [4, 5]. It was discussed that

this collective deformation is originated from the strong attractive interaction between protons and neutrons [6]. Here, atomic nuclei are deformed as a whole, resulting in a strong enhancement in the transition probability from the first excited state to the ground state. This is in marked contrast to trivial deformation seen in nuclei with a valence nucleon outside a doubly-magic nucleus [7–10]. Since doubly-magic nuclei are, in general, spherical, such deformation is entirely due to the valence nucleon, thus of single-particle nature, unless the valence nucleon induces a strong polarization effect of the core nucleus [11]. Although some of such atomic nuclei are known to be deformed beyond single-particle level, the collective deformation is known to be much more significant than such a single-particle deformation. We note that atomic nuclei may also be deformed due to the α -cluster formation [12–22], even though it is out of the scope of this paper. See Refs. [4, 5] for more details.

A natural question then arises: Can atoms be deformed collectively as in atomic nuclei? Notice that calculations of the atomic structure have been usually carried out by assuming spherical symmetry [23–25], and the non-sphericity has been taken care of only in a few works [26, 27]. Likewise, spherical symmetry has been usually assumed to construct the pseudopotential for valence electrons in calculations of molecules and solids [28–31]. It is thus widely believed that atoms are rather spherical, in stark contrast to deformed atomic nuclei. What is the physical origin of this difference? To what extent can electron distributions in atoms be deformed collectively?

To answer these questions, in this paper we calculate electron distributions of atoms and their deformation parameters using various numerical methods without assuming spherical symmetry. Namely, we use and compare the unrestricted Hartree-Fock method [32–36], several post-Hartree-Fock methods [36–48], and the density functional theory [49–51]. By estimating the change in the energy induced by the deformation, in nuclear systems, we find that the spin-up and spin-down particles tend to be deformed in the same manner due to the attractive inter-particle nuclear interaction. In atomic systems, on the other hand, we find that the spin-up and spin-down particles prefer to be deformed in the opposite manner, cancelling each other and resulting in a small deformation as a whole due to the repulsive inter-particle Coulomb interaction. We, thus, show that the difference between atoms and atomic nuclei on their deformability primarily originates from the different nature of the inter-particle interactions.

The paper is organized as follows. In Sec. 2, we first detail the deformation of many-body systems, and introduce a parameter β to characterize the deformation. We then carry out numerical calculations for isolated atoms and discuss their deformations in Sec. 3. In Sec. 4, we qualitatively compare between atoms and nuclei using a model to estimate a change in the energy, and discuss the origin for collective deformation. We then summarize the paper in Sec. 5. In Appendix A, we discuss the deformation of neutron drops, that is, many-neutron systems trapped in a harmonic oscillator potential, and exemplify that nuclear systems can be deformed collectively. In Appendix B, a generalization of the calculations in Sec. 4 is presented. Appendix C summarizes the numerical data for atomic deformation calculated in the main part of the paper.

2. Collective deformation of many-fermion systems

2.1. Deformation parameters

Before we present the results of our calculations, let us briefly summarize the basic concepts of collective deformation. Atomic nuclei in the rare earth region, such as ^{154}Sm and ^{168}Er , as well as those in the actinide region, such as ^{234}U , often exhibit characteristic spectra, in which the energy of the state with the total angular momentum I ($I = 0, 2, 4, \dots$) is proportional to $I(I + 1)$. These spectra are interpreted as that those nuclei are deformed in the ground state and show the rotational spectra given by

$$E_{\text{rot}} = \frac{I(I + 1)\hbar^2}{2\mathcal{I}}, \quad (2.1)$$

where \mathcal{I} is the moment of inertia for the rotational motion. An important fact is that a large number of nucleons in those nuclei are involved in the deformation, and thus such deformation is referred to as collective deformation. Indeed, the electromagnetic transition probability from e.g., the $I = 2$ state to the $I = 0$ state (i.e., the ground state) is significantly enhanced due to the collectivity of deformation [5].

The collective deformation is characterized by a non-zero value of the quadrupole moment Q_{ij} defined by

$$Q_{ij} = \int (3r_i r_j - \delta_{ij} r^2) \rho(\mathbf{r}) d\mathbf{r} \quad (i, j = x, y, z), \quad (2.2)$$

where $\rho(\mathbf{r})$ is the density distribution. Note that there exist several normalizations for the quadrupole moment tensor Q . Here, we take the normalization often used in nuclear physics [5], which is sometimes referred to as ‘‘traceless quadrupole moment’’ in the context of quantum chemistry.

The symmetric matrix Q_{ij} can be diagonalized to define the cartesian axes, x' , y' , and z' in the intrinsic frame. With the eigenvalues of Q_{ij} , the deformation parameters β_k can be defined as

$$\beta_k = \sqrt{\frac{\pi}{5}} \frac{Q_k}{N_{\text{tot}} \langle r^2 \rangle} \quad (k = x', y', z'), \quad (2.3)$$

where Q_k is an eigenvalue of Q_{ij} and $\langle r^2 \rangle$ is the mean-square radius given by

$$\langle r^2 \rangle = \frac{\int r^2 \rho(\mathbf{r}) d\mathbf{r}}{\int \rho(\mathbf{r}) d\mathbf{r}} = \frac{1}{N_{\text{tot}}} \int r^2 \rho(\mathbf{r}) d\mathbf{r}, \quad (2.4)$$

with N_{tot} being the total number of particle in the system. For atoms, N_{tot} is the total number of electrons (the atomic number), Z , whereas for atomic nuclei it is the total number of nucleons (the mass number), A .

The deformation parameter β_j is closely related to the angle-dependent radius of the system, $R(\theta, \phi)$. The radius can be expanded in multipoles with spherical harmonics Y_{lm} as [5]

$$R(\theta, \phi) = R_0 \left[1 + \sum_{l=2}^{\infty} \sum_{m=-l}^l a_{lm} Y_{lm}^*(\theta, \phi) \right]. \quad (2.5)$$

The monopole part ($l = 0$) in the expansion is absorbed in the definition of R_0 , while the dipole part ($l = 1$) need not be considered since, to the first order, it merely shifts the center

of mass of the whole system without changing its shape. If one considers only the quadrupole deformation with $l = 2$, after transforming to the intrinsic frame, Eq. (2.5) is reduced to

$$\begin{aligned} R(\theta', \phi') &= R_0 \left[1 + \beta \cos \gamma Y_{20}(\theta', \phi') + \frac{1}{\sqrt{2}} \beta \sin \gamma Y_{22}(\theta', \phi') + \frac{1}{\sqrt{2}} \beta \sin \gamma Y_{2-2}(\theta', \phi') \right] \\ &= R_0 \left[1 + \sqrt{\frac{5}{16\pi}} \beta \left\{ \cos \gamma (3 \cos^2 \theta' - 1) + \sqrt{3} \sin \gamma \sin^2 \theta' \cos 2\phi' \right\} \right], \end{aligned} \quad (2.6)$$

with $a'_{20} = \beta \cos \gamma$, $a'_{22} = a'_{2-2} = \frac{1}{\sqrt{2}} \beta \sin \gamma$, and $a'_{21} = a'_{2-1} = 0$, where the primes denote the quantities in the intrinsic frame. Here, $\beta > 0$ and γ represent the degrees of elongation and triaxiality [5]. Due to the symmetry, γ can be restricted to $\gamma \in [0, \pi/3]$. In addition, $\gamma = \pi/3$ with $\beta > 0$ is identical to $\gamma = 0$ with $\beta < 0$. Hence, if one only considers the axially symmetric case with both positive and negative β , Eq. (2.6) can be simplified further as

$$R(\theta', \phi') = R_0 \left[1 + \sqrt{\frac{5}{16\pi}} \beta (3 \cos^2 \theta' - 1) \right], \quad (2.7)$$

with axially symmetric shape about the z' axis. In this case, the radii in the x' , y' , and z' directions are given by

$$R_{x'} = R_{y'} = R(\pi/2, \phi') = R_0 \left(1 - \sqrt{\frac{5}{16\pi}} \beta \right), \quad (2.8)$$

$$R_{z'} = R(0, \phi') = R_0 \left(1 + 2\sqrt{\frac{5}{16\pi}} \beta \right), \quad (2.9)$$

respectively. Thus, the density distribution is spherical for $\beta = 0$, while for $\beta > 0$ and $\beta < 0$ it becomes prolate and oblate shapes, respectively, as shown in Fig. 1. For a positive value of β , the z' axis makes the longest axis as shown schematically in Fig. 2.

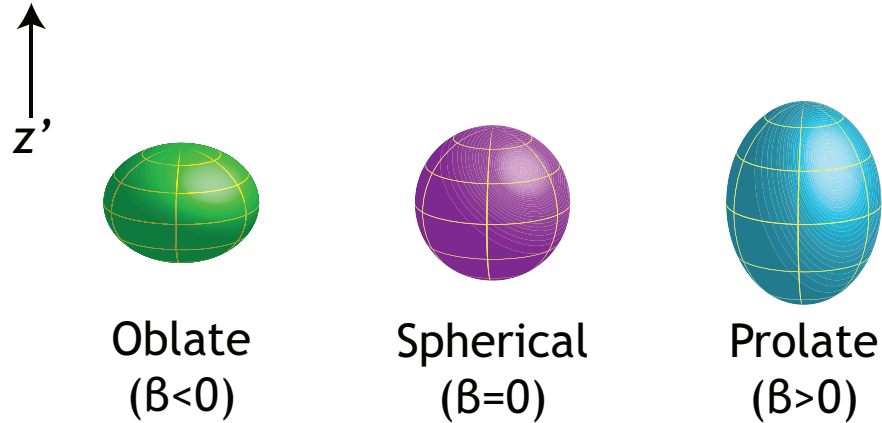


Fig. 1 A schematic picture of the collective deformation.

The quadrupole deformation parameter β here corresponds to β_z defined by Eq. (2.3) (to the leading order, at least for a sharp-cut density distribution with the radius $R(\theta, \phi)$ [5]). Note that the condition of $Q_x = Q_y = -Q_z/2$, i.e., $\beta_x = \beta_y = -\beta_z/2 = -\beta/2$, holds for the axially symmetric case.

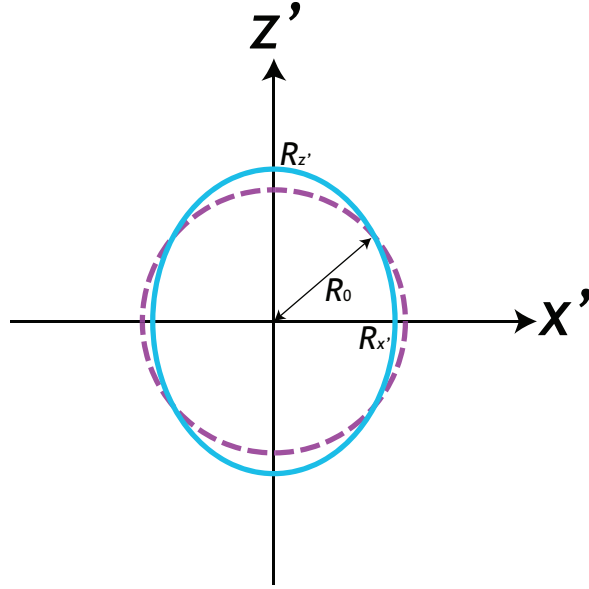


Fig. 2 A schematic picture of a collective deformation in the $x'z'$ plane defined in the intrinsic frame. The axially symmetric shape along the z' axis is assumed. The dashed and the solid curves correspond to the deformation parameter of $\beta = 0$ and 0.25, respectively.

If the particles in different spin states undergo different deformations, as in the case for the electrons in atoms to be discussed in Sec. 4, spin-dependent deformation parameters β_{\uparrow} and β_{\downarrow} can be also defined. Since $\rho(\mathbf{r}) = \rho_{\uparrow}(\mathbf{r}) + \rho_{\downarrow}(\mathbf{r})$ holds, $Q = Q_{\uparrow} + Q_{\downarrow}$ also does, where ρ_{\uparrow} and ρ_{\downarrow} denote the densities of up-spin and down-spin fermions, respectively.

It should also be noted that the discussion here is based on the intrinsic frame. In the laboratory frame, there is no criterion to choose the symmetry axis (that is, the z axis) and the system would show spherical distribution, even when it is deformed in the intrinsic frame.

Microscopically, the collective deformation discussed in this section is intimately related to the mean-field theory. In this theory, particles move independently in a mean field potential, which is formed self-consistently by the interaction among the particles. The collective deformation occurs as a consequence of spontaneous breaking of rotational symmetry. That is, a system may be *intrinsically* deformed and breaks the rotational symmetry even if the total Hamiltonian has the symmetry. This is actually a good advantage of the self-consistent mean-field theory used in Sec. 3, since a large part of the many-body correlations can be taken into account while keeping the simple picture of independent particles [5, 52–54].

2.2. Single-particle contribution to deformation

In connection to the deformation in atoms discussed in the next section, it is instructive to compute the deformation parameters discussed in the previous subsection for a system with a spherical core plus a valence particle. In this case, the quadrupole moment of the system entirely comes from the valence particle, since Eq. (2.2) vanishes for the spherical density distribution. If one assumes that the wave function for the valence particle is given by

$$\psi_{nlms}(\mathbf{r}) = \frac{u_{nl}(r)}{r} Y_{lm}(\theta, \phi) \chi_s, \quad (2.10)$$

as a single-particle orbital in a spherical (effective) potential, where χ_s is the spinor of the valence particle, the quadrupole moments of the whole system read $Q_{ij} = q_{ij}^{(\text{sp})}$ with

$$\begin{aligned} q_{ij}^{(\text{sp})} &= \int (3r_i r_j - \delta_{ij} r^2) |\psi_{nlms}(\mathbf{r})|^2 d\mathbf{r} \\ &= \int (3\mathfrak{s}_i \mathfrak{s}_j - \delta_{ij}) r^2 |\psi_{nlms}(\mathbf{r})|^2 d\mathbf{r}. \end{aligned} \quad (2.11)$$

Here, we have introduced the notation $r_i = r\mathfrak{s}_i$ with

$$\mathfrak{s}_i = \begin{cases} \sin \theta \cos \phi & (i = x), \\ \sin \theta \sin \phi & (i = y), \\ \cos \theta & (i = z). \end{cases} \quad (2.12)$$

Substituting Eq. (2.10), one finds

$$q_{ij}^{(\text{sp})} = \int_0^\infty r^2 |u_{nl}(r)|^2 dr \int (3\mathfrak{s}_i \mathfrak{s}_j - \delta_{ij}) |Y_{lm}(\theta, \phi)|^2 d\Omega, \quad (2.13)$$

where $d\Omega$ is the angular part of $d\mathbf{r}$. Note that the off-diagonal components of $q_{ij}^{(\text{sp})}$ vanish. The deformation parameter for the valence particle, that is, the single-particle deformation parameter, then reads,

$$\beta_i^{(\text{sp})} = \sqrt{\frac{\pi}{5}} \frac{q_{ii}^{(\text{sp})}}{\langle r^2 \rangle_{nl}} = \sqrt{\frac{\pi}{5}} \int (3\mathfrak{s}_i^2 - 1) |Y_{lm}(\theta, \phi)|^2 d\Omega. \quad (2.14)$$

Notice that the radial integral in Eq. (2.13) is cancelled with the mean-square radius

$$\langle r^2 \rangle_{nl} = \int_0^\infty r^2 |u_{nl}(r)|^2 dr. \quad (2.15)$$

The deformation parameter of the whole system (i.e., the core plus the valence particle) is then given by

$$\beta_i = \sqrt{\frac{\pi}{5}} \frac{q_i^{(\text{sp})}}{N_{\text{tot}} \langle r^2 \rangle}, \quad (2.16)$$

where $\langle r^2 \rangle = [(N_{\text{tot}} - 1) \langle r^2 \rangle_{\text{core}} + \langle r^2 \rangle_{nl}] / N_{\text{tot}}$ is the mean-square radius of the whole system with $\langle r^2 \rangle_{\text{core}}$ being that of the core. If one assumes the radius of the whole system is similar to the radius of the valence orbital, $\langle r^2 \rangle \simeq \langle r^2 \rangle_{nl}$, which is reasonable in the case of atomic nuclei, the deformation parameter is given by

$$\beta_i \simeq \frac{\beta_i^{(\text{sp})}}{N_{\text{tot}}}. \quad (2.17)$$

In contrast, in the case of atoms, valence electrons have a larger spatial distribution and contribute more significantly than inner core electrons to the radius $\langle r^2 \rangle$. If one assumes

$\langle r^2 \rangle \simeq \langle r^2 \rangle_{nl} / N_{\text{tot}}$, i.e., only one electron mainly contributes to $\langle r^2 \rangle$, one obtains

$$\beta_i \simeq \beta_i^{(\text{sp})}. \quad (2.18)$$

Notice that when the number of valence electrons is N_{val} , the deformation parameter is, instead, approximately given by

$$\beta_i \simeq \frac{\sum_{\text{val}} \beta_i^{(\text{sp})}}{N_{\text{val}}}. \quad (2.19)$$

Let us evaluate explicitly the single-particle deformation parameter for the pure p and d orbitals. To this end, we define the indices of the real spherical harmonics as follows [55]:

$$Y_p^x(\theta, \phi) = \sqrt{\frac{3}{4\pi}} \sin \theta \cos \phi, \quad (2.20a)$$

$$Y_p^y(\theta, \phi) = \sqrt{\frac{3}{4\pi}} \sin \theta \sin \phi, \quad (2.20b)$$

$$Y_p^z(\theta, \phi) = \sqrt{\frac{3}{4\pi}} \cos \theta, \quad (2.20c)$$

and

$$Y_d^{xy}(\theta, \phi) = \sqrt{\frac{15}{16\pi}} \sin^2 \theta \sin 2\phi, \quad (2.21a)$$

$$Y_d^{yz}(\theta, \phi) = \sqrt{\frac{15}{16\pi}} \sin 2\theta \sin \phi, \quad (2.21b)$$

$$Y_d^{zx}(\theta, \phi) = \sqrt{\frac{15}{16\pi}} \sin 2\theta \cos \phi, \quad (2.21c)$$

$$Y_d^{x^2-y^2}(\theta, \phi) = \sqrt{\frac{15}{16\pi}} \sin^2 \theta \cos 2\phi, \quad (2.21d)$$

$$Y_d^{z^2}(\theta, \phi) = \sqrt{\frac{5}{16\pi}} (3 \cos^2 \theta - 1). \quad (2.21e)$$

Using these notations, the deformation parameter $\beta_i^{(\text{sp})}$ for Y_p^j is found to be

$$\beta_i^{(\text{sp})} = \begin{cases} \frac{4}{5} \sqrt{\frac{\pi}{5}} = 0.6341 & (i = j), \\ -\frac{2}{5} \sqrt{\frac{\pi}{5}} = -0.3171 & (\text{Otherwise}). \end{cases} \quad (2.22)$$

For the d -orbitals, the deformation parameter for Y_d^{jk} ($(j, k) = (x, y), (y, z), (z, x)$) is given by

$$\beta_i^{(\text{sp})} = \begin{cases} -\frac{4}{7} \sqrt{\frac{\pi}{5}} = -0.4530 & (i \neq j \text{ and } i \neq k), \\ \frac{2}{7} \sqrt{\frac{\pi}{5}} = 0.2265 & (\text{Otherwise}), \end{cases} \quad (2.23a)$$

while the deformation parameters for $Y_d^{x^2-y^2}$ and $Y_d^{z^2}$ read

$$\beta_i^{(\text{sp})} = \begin{cases} -\frac{4}{7} \sqrt{\frac{\pi}{5}} = -0.4530 & (i = z), \\ \frac{2}{7} \sqrt{\frac{\pi}{5}} = 0.2265 & (\text{Otherwise}), \end{cases} \quad (2.23b)$$

and

$$\beta_i^{(\text{sp})} = \begin{cases} \frac{4}{7} \sqrt{\frac{\pi}{5}} = 0.4530 & (i = z), \\ -\frac{2}{7} \sqrt{\frac{\pi}{5}} = -0.2265 & (\text{Otherwise}), \end{cases} \quad (2.23c)$$

respectively. Note that due to higher-order deformations, the d orbitals are not axially symmetric except the d_{z^2} orbital, even though triaxiality vanishes ($\gamma = 0$).

3. Numerical Calculation

In this section, a possibility of the deformation of isolated atoms is studied numerically with the computational code GAUSSIAN [56]. In the GAUSSIAN code, the wave function and the energy of the ground state of atomic and molecular systems are numerically calculated by using the Gaussian-type basis expansion. With this code, all-electron calculation can be performed for a wide range of atoms ($Z \leq 54$).

First, our calculation setup is explained in Sec. 3.1. Then, the results and their basic explanations are presented in Secs. 3.2 and 3.3, where we shall see that open-shell atoms have non-zero deformation parameters. To understand clearly the mechanism of such deformations, we discuss the results in more details in Sec. 3.4 by analyzing the deformations of each single-particle orbital. Finally, a short summary of the numerical results and their physical explanations will be presented in Sec. 3.5.

For convenience, the Hartree atomic unit $m_e = \hbar = e^2 = a_B = 4\pi\epsilon_0 = 1$ is used, where m_e is the mass of electrons, ϵ_0 is the permittivity of vacuum, and $a_B = 5.2918\dots \times 10^{-11}$ m is the Bohr radius [57, 58]. The unity of the electric quadrupole moment in the Hartree atomic unit corresponds to $4.4866\dots \times 10^{-40}$ C m² = 1.3450... Debye Å. Here, we use quadrupole moment of *density* itself, instead of *charge* density, and thus Q_k in this paper corresponds to $-e$ (< 0) times of the electric quadrupole moment.

3.1. Calculation setup and deformation parameters

An isolated neutral atom with the atomic number Z in the non-relativistic scheme is described by the Hamiltonian

$$H = -\frac{1}{2} \sum_{j=1}^Z \Delta_j + \sum_{j=1}^Z V_{\text{ext}}(\mathbf{r}_j) + \sum_{1 \leq j < k \leq Z} V_{\text{int}}(\mathbf{r}_j, \mathbf{r}_k), \quad (3.1)$$

where \mathbf{r}_j is the coordinate of the particle j . The external potential V_{ext} and the electron-electron interaction V_{int} read

$$V_{\text{ext}}(\mathbf{r}) = -\frac{Z}{r}, \quad (3.2)$$

$$V_{\text{int}}(\mathbf{r}_j, \mathbf{r}_k) = \frac{1}{r_{jk}}, \quad (3.3)$$

respectively, where $r = |\mathbf{r}|$ and $r_{jk} = |\mathbf{r}_j - \mathbf{r}_k|$. Here, the atomic nucleus is assumed to be a point charge and the spin-orbit interaction is neglected.

In this paper, the many-body Schrödinger equation is approximately solved using mainly the unrestricted Hartree-Fock (UHF) method [32–36]. To assess the dependence of the many-body methods, several post-Hartree-Fock methods and the density functional theory [49–51] with the PZ81 local density approximation (LDA) exchange-correlation functional [59] are also employed. As for the post-Hartree-Fock methods, we choose the configuration interaction [41, 42, 44, 48] with double excitations (CID) and single-double excitations (CISD), the coupled-cluster method [38–40] with double excitations (CCD) and single-double excitations (CCSD), and Møller-Plesset many-body perturbation theory [37] with second (MP2), third

(MP3), and fourth (MP4) orders [43, 45–47]. For the MP4 calculation, the excitations are restricted to single, double, and quadruple excitations (MP4SDQ), which is simply referred to as MP4. The calculations are performed with these post Hartree-Fock methods, i.e., CID, CISD, CCD, CCSD, MP2, MP3, and MP4, based on the UHF calculation. In these post Hartree-Fock calculations, the core is not treated as frozen.

To perform the many-body calculations, the basis expansions with the 6-31+G [60, 61], dAug-CC-pV5Z [62, 63], and STO-3G [64] bases are used. It should be noted that the different bases are optimized to different ranges of atoms: The STO-3G basis can be applied from H atom to Xe atom. The applicable ranges of the 6-31+G and the dAug-CC-pV5Z bases are limited to atoms from H to Kr. In addition, the dAug-CC-pV5Z basis cannot be applied to Mg, K, or Ca atoms.

After we obtain the electron density $\rho(\mathbf{r})$ with these numerical methods, the mean-square radius $\langle r^2 \rangle$ and the quadrupole moments Q_i are calculated according to Eqs. (2.2) and (2.4), respectively. Here, we define the coordinate frame so that the quadrupole moment tensor Q is diagonalized (see Eq. (2.3)).

To perform the calculation with the GAUSSIAN code, the multiplicity of the ground states has to be assumed, which are taken from the database provided by the National Institute of Standards and Technology (NIST) [65]. We do not assume any symmetry for the initial condition, nor use the filling approximation, in which valence orbitals in open shells are filled with equal occupation probabilities¹. With this procedure, non-spherical electron density can be described properly. After the calculation is converged, the valence-electron configurations are evaluated by using the natural orbital analysis [66–69].

In this paper, we mainly employ the 6-31+G basis, while the results with the dAug-CC-pV5Z and STO-3G bases are also shown in Appendix C.

3.2. Systematic behaviors of atomic deformations and their basis dependence

Let us now numerically investigate deformation in atoms. We first show in Fig. 3 the deformation parameter β for atoms from Li ($Z = 3$) to Kr ($Z = 36$) calculated with the unrestricted Hartree-Fock method with the 6-31+G basis. See Table C1 in Appendix C for the actual values. In Fig. 3, we use different symbols to classify the nature of the atoms: The filled circles show noble-gas (i.e., closed-shell) atoms. The filled squares show half-closed-shell atoms; atoms with three valence electrons occupying the outer-most p orbitals, or with five valence electrons occupying the outer-most d orbitals. The triangles, the inverse triangles, and the diamonds show the others; atoms with s , p , and d orbitals for the outer-most open shell, respectively [70]. Note that the octupole moments for all the calculated atoms are found to be zero.

Spherical atoms—According to Fig. 3, all the noble-gas atoms are spherical ($\beta = 0$), as is expected. Such trivial results are guaranteed by the fact that all the orbitals for any given principal and azimuth quantum numbers, n and l , are either fully occupied or unoccupied,

¹ For example, in the case of B, $2p_x$, $2p_y$, and $2p_z$ orbitals are occupied with the probability of 1/3. Notice that the wave function in the filling approximation is different from the coherent superposition of those orbitals, $|\text{val}\rangle = (|2p_x\rangle + |2p_y\rangle + |2p_z\rangle) / \sqrt{3}$, even though both of them lead to a spherical density distribution.

and thus their distributions are, in total, spherical. In other words, $\sum_{m=-l}^l |Y_{lm}(\theta, \phi)|^2 = (2l + 1)/4\pi$ is a constant, independent of the angles θ and ϕ .

For the other atoms, the electronic configuration of their cores is the same as that of the noble-gas atoms. Hence, as long as the core density is not deformed due to non-trivial many-body effects, i.e., the polarization due to the interaction between the core and valence electrons, the deformation of the atom is expected to come only from the valence electrons. Possibility of such non-trivial deformation will be studied in details in Sec. 3.4, but we can easily conclude before going to such details that the s -block and half-closed-shell atoms should be spherical ($\beta = 0$), as shown in Fig. 3. The valence electrons of the s -block atoms by definition only occupy an s orbital, and the many-body effects between the valence electrons and the spherically symmetric core necessarily results in a spherical electron distribution. This is the case also for the half-closed-shell atoms: Atom with three electrons occupying valence p orbitals, or those with five electrons occupying valence d orbitals, are spherical in both cases, since α -spin electrons occupy all the $(2l + 1)$ states with $m = -l, -l + 1, \dots, l$ due to the Hund rule [71–75].

Open-shell atoms—For the other open-shell atoms (p -block and d -block atoms), the deformation parameters β are generally non-zero. The deformation parameters for the atoms with the same group show similar tendencies, i.e., $|\beta| \simeq 0.1$ – 0.3 for the p -block atoms and $|\beta| \lesssim 0.01$ for the d -block atoms. This shows that the nature of the few valence open-shell electrons plays a major role in determining β of the whole atom. In the context of nuclear physics, an atomic nucleus with the deformation parameter of $\simeq \pm 0.1$ or larger is regarded as a deformed nucleus (see Appendix A). It is thus tempting to regard the atoms with $|\beta| \gtrsim 0.1$ as significantly deformed as nuclei. However, this deformation originates from single-particle valence orbitals and thus it is misleading to regard it as collective deformation. For example, the deformation of the p -block atoms can be understood as the valence p orbitals mainly contributing to the deformation. Indeed, $|\beta| \simeq 0.1$ – 0.3 of the p -block atoms in Fig. 3 are similar values in order of magnitude as that of a single p orbital given by Eqs. (2.18) and (2.22). On the other hand, the deformations of the d -block atoms are much smaller than those of the p -block atoms (see and compare with Eq. (2.23)). This implies that one cannot regard the deformation of d -block atoms as originating only from the single-orbital deformation. The mechanism of the deformation and the physical origin of this difference will be discussed in Sec. 3.4: We will conclude there that the p -block atoms can be regarded as an almost inert core plus valence p -electrons, while many-body effects between the core and the valence electrons are relevant in the d -block atoms. In the d -block atoms, the core electrons tend to collectively cancel the deformation of the valence d orbitals.

Exceptionally $\beta = 0$ open-shell atoms are V ($Z = 23$), Co ($Z = 27$), Cu ($Z = 29$), and Zn ($Z = 30$). In the case of Cu and Zn atoms, ten of the valence electrons completely occupy the valence d orbital and the remaining one or two valence electrons occupy the s orbital. Thus, they are trivially spherical, in the same manner as the s -block atoms. In the case of V and Co atoms, on the other hand, three or eight valence electrons occupy the d orbitals. At first sight, such open-shell d -block atoms do not seem to be trivially $\beta = 0$. However, we note that they can be $\beta = 0$ if $d_{x^2-y^2}$ and d_{z^2} orbitals are occupied (unoccupied) at the same

time ². For example, d^8 occupation may lead to $\beta = 0$ if the unoccupied orbitals are $d_{x^2-y^2}$ and d_{z^2} orbitals. This is the case for Co atom. For V atom, d^3 occupation leads to $\beta = 0$ because $d_{x^2-y^2}$ and d_{z^2} orbitals are occupied simultaneously.

Basis dependence—In order to guarantee that our results presented in this section and in Fig. 3 do not depend on a specific choice of the basis in the calculation, we repeat calculations with different basis sets: In addition to the 6-31+G basis used in Fig. 3 and Table C1 in Appendix C, we also use the dAug-CC-pV5Z and STO-3G bases. The results are shown in Table C2 and Table C3 in Appendix C, respectively. We find that as long as the configurations of the valence electrons are the same, the deformation parameters β are essentially the same, hence basis independent. We note, however, that there are a few results with the STO-3G basis which are different from those with the dAug-CC-pV5Z and 6-31+G bases, even when the configurations are the same. This may be because the STO-3G basis set spans a smaller space than the other basis sets, and thus the tail region of the electron density distribution $\rho(\mathbf{r})$ is not accurately described compared with the others.

3.3. Many-body method dependence

Our results presented in the previous section essentially remain the same, even if we employ other many-body methods than the unrestricted Hartree-Fock (UHF) method. As benchmark examples, Al ($Z = 13$), Cu ($Z = 29$), and Ga ($Z = 31$) are selected. In Fig. 4, we show the deformation parameters β for those atoms calculated with a wide variety of different many-body methods with the 6-31+G basis. The data are shown in Table C4 in Appendix C. We find that the deformation parameters β calculated with the post-Hartree-Fock methods (CCD, CCSD, CID, CISD, MP2, MP3, and MP4) are almost the same as those with the UHF. The excellent agreement of the UHF and the post-Hartree-Fock methods in Fig. 4 implies that the correlations beyond Hartree-Fock may be irrelevant to the quadrupole deformation.

We have also performed the DFT calculation (indicated by LDA in Fig. 4) and found that the result also agrees excellently with the UHF and post-Hartree-Fock methods. Since the DFT method is not directly linked to the UHF calculation, there is no *a priori* reason why β should be the same. In principle, owing to the Hohenberg-Kohn theorem, the DFT calculation provides the exact, i.e., the full CI, density, if the exact exchange-correlation functional were known. In practice, the DFT results should depend on the choice of the employed exchange-correlation functional, since only approximated functional have been known. The excellent agreement between the DFT (LDA) and the other methods in Fig. 4, therefore, guarantees that finite deformation parameters presented in the previous section and following sections are not at all artifacts of a specific many-body approximation method.

We note that all the above results and discussions in this section hold true for the other bases: We have performed the same calculation also with dAug-CC-pV5Z basis as shown in Table C5 in Appendix C, and obtained essentially the same results as those with the 6-31+G basis in Fig. 4 and Table C4.

² Higher-order deformations, such as hexadecapole deformation, exist even though they are considerably small.

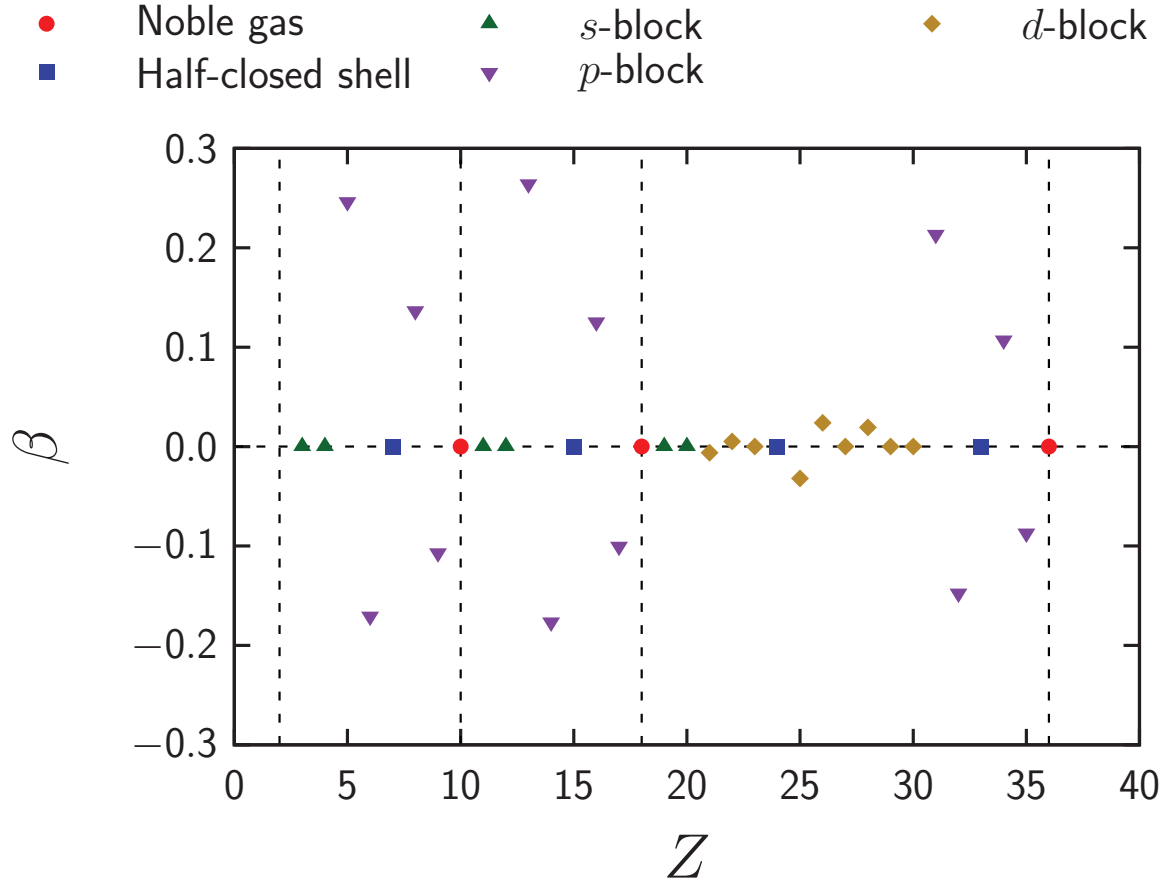


Fig. 3 Deformation parameter β as a function of the atomic number Z calculated with the unrestricted Hartree-Fock method with the 6-31+G basis. The filled circles and the filled squares show noble-gas and half-closed-shell atoms, respectively. The triangles, the inverse-triangles, and the diamonds show the others: atoms with the outer-most open-shell s orbitals (s block), p orbitals (p block), and d orbitals (d block), respectively. The vertical dashed lines denote the closed-shell atoms.

3.4. Analyses with single-particle orbitals

To understand further the physical mechanism of the atomic deformations, let us define the deformation parameter of each single-particle orbital $\beta_{\max}^{(\text{sp})}$ by $\beta_i^{(\text{sp})}$ for the direction of the symmetry axis of the orbital. Here, the symmetry axis of the orbital may be different from that of the whole atoms, i.e., the i axis for p_i orbital, the k axis for d_{ij} orbital ($i \neq j \neq k$), and the z axis for the other d orbitals. Angular-momentum mixing can occur due to the deformation, so that single-particle orbitals in these methods can, in general, show β different from those of the pure spherical harmonics. Specifically, as we will see, an s orbital can show a non-zero β due to the mixture with d orbitals. Note that $\beta_{\max}^{(\text{sp})}$ is the deformation parameter for each single-particle orbital (see Eq. (2.14)), which is divided by the radius of each orbital. Therefore, β_i of the whole atom is not a simple sum of $\beta_{\max}^{(\text{sp})}$. Thus, a care must be taken when using them, but they are still useful in understanding the mechanism of the deformation microscopically.

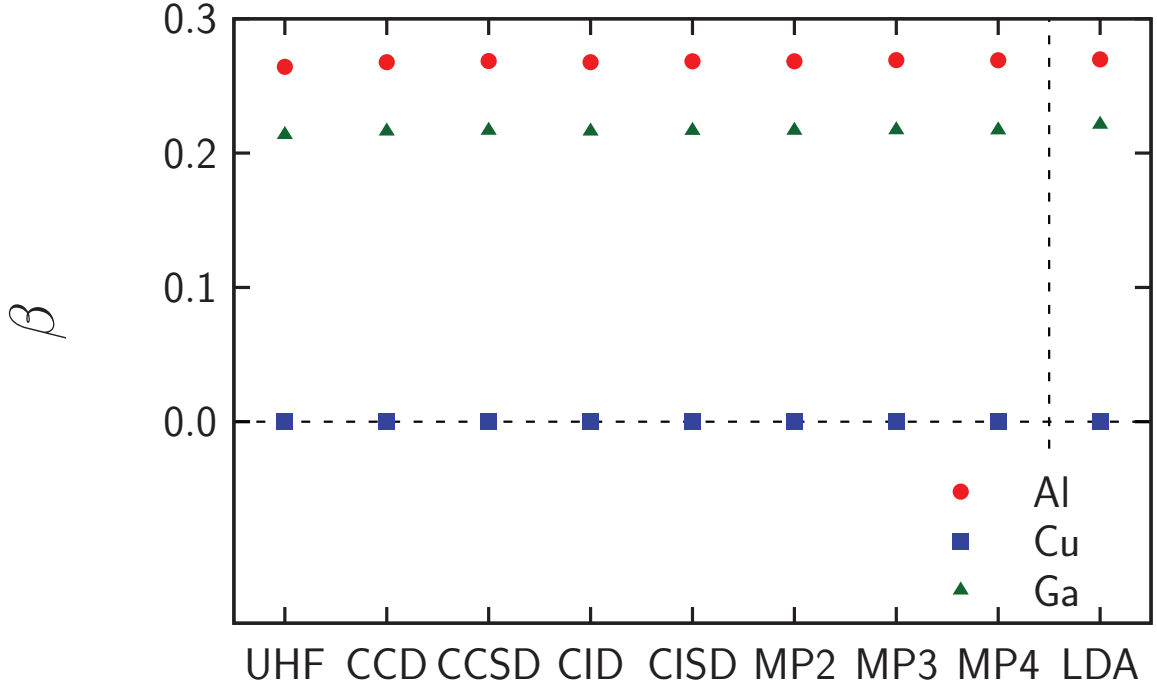


Fig. 4 Dependence of the deformation parameter β on many-body methods with the 6-31+G basis. Data for Al ($Z = 13$), Cu ($Z = 29$), and Ga ($Z = 31$) are shown with circles, squares, and triangles, respectively. For more details, see the text.

Deformation of single-particle orbitals—Table 1 shows $\beta_{\max}^{(\text{sp})}$ for selected valence orbitals of some open-shell atoms. All the data are calculated by the unrestricted Hartree-Fock calculation with the 6-31+G basis. First, we find that the deformation parameters of the valence p and d orbitals are almost the same as those of the pure p and d orbitals given by Eqs. (2.22)–(2.23c). This suggests that even when the atom is deformed, the single-particle orbitals of the valence p and d electrons are described almost as a product of the radial function and the pure spherical harmonics. In other words, the valence p and d electrons feel an almost perfectly spherical effective (Hartree-Fock or Kohn-Sham) potential. We can, therefore, conclude that the density of the electrons is almost perfectly spherical in the central region due to the strong Coulomb force of the nucleus, resulting in the spherical effective potential for the valence electrons. The electron density is deformed only in the surface and the tail regions of the atoms described by the valence electrons.

Deformations in the surface and degeneracy lifting—Such deformations lead to a non-spherical effective potential in the surface and the tail regions. There are several evidences for this. Firstly, the outer-most s orbital can have non-zero β and become non-spherical. This is shown in Table 1 as a non-zero β of the $4s$ orbitals, which tend to cancel the deformation of the valence $3d$ orbitals. This is due to the screening effect. That is, the outer-most $4s$ electrons try to cancel the deformed electron density of the open-shell valence $3d$ electrons. We will discuss this s -orbital deformation in more details later in this section taking Sc atom as an example.

Secondly, the orbitals with the same n and l become non-degenerate in energy in some cases. This can be seen in Table 2, where the quadrupole moment of $q_{\max}^{(\text{sp})}$, the square radius

$\langle r^2 \rangle$, and the eigenenergies of the single-particle orbitals ε_j , for Sc atoms are shown. As one can see, the eigenenergies of the p_z states become different from those of p_x and p_y states. Since the deformation is axially symmetric and thus there is only one specific direction, i.e., the orbitals along x and y axes (p_x and p_y orbitals or d_{yz} and d_{zx} orbitals) remain degenerate. This is similar to the Stark effect [76]. We note, however, that the energy difference for the core orbitals is the order of 0.05 Hartree $\simeq 1$ eV or less, and is rather small. This is because they have small overlap with the valence wave functions creating the non-spherical effective potential.

On the other hand, for the open-shell outer-most valence electrons, such liftings of degeneracy can be relevant. For example, the outer-most electron of Al atom occupies the $3p_z$ orbital. If the system is completely spherical, the $3p_z$ orbital is degenerate with the $3p_x$ and $3p_y$ orbitals, while due to the deformation the $3p_x$ and $3p_y$ orbitals are non-degenerate to the $3p_z$ orbital. The eigenenergy of the $3p_z$ orbital is -0.2099 Hartree, while those of the $3p_x$ and $3p_y$ orbitals are 0.0121 Hartree. Due to this degeneracy lifting, the last electron prefers to occupy the $3p_z$ orbital instead of the equal filling of the $3p_x$, $3p_y$, and $3p_z$ orbitals, leading to the deformation. It is noted that this degeneracy lifting of p states results from the second-order perturbation: It is caused by the deformation of the core and the $3s$ orbital, which is induced by the existence of the $3p_z$ electron.

These results suggest that the dominant part of the effective potential is created by the spherical central region. The non-spherical contribution to the effective potential of the valence deformed electrons is sub-dominant and can be treated as small correction.

Screening effect—Let us scrutinize deformations of each orbital with Sc ($Z = 21$) atom in Table 2 (results for other atoms are also shown in Table C6–C10 in Appendix C). Here, Sc atom has filled $1s$ – $3p$ orbitals, in addition to one $3d_{xy}$ electron and two $4s$ electrons. The quadrupole moments $q_z^{(\text{sp})}$ of the filled $1s$ – $3p$ orbitals completely cancel each other, resulting in undeformed spherical core. The square radii of the $1s$ – $3p$ orbitals are much smaller than those of $3d_{xy}$ and $4s$ orbitals, so that we can essentially regard Sc atom as a system of one $3d_{xy}$ electron and two $4s$ electrons orbiting around an almost perfectly inert small spherical core. The electron in the $3d_{xy}$ in the α -spin state is oblate $q_z^{(\text{sp})} = -2.1642 < 0$. This results in an oblate shape of Sc atom as a whole, but the value $q_z^{(\text{sp})} = -0.4189$ is much smaller than the quadrupole moment of the $3d_{xy}$ electron. This can be explained by the screening effect: We can see in Table 2 that the electron in the $4s$ orbital with β -spin state deforms so significantly that the quadrupole moment of the $\beta 4s$ electron cancels that of the $\alpha 3d_{xy}$ orbital. To be more precise, $|q_z^{(\text{sp})}|$ of $\beta 4s$ is almost the same but slightly smaller than $|q_z^{(\text{sp})}|$ of $\alpha 3d_{xy}$, which suggests that the quadrupole moment of the $\alpha 3d_{xy}$ electron is almost but not perfectly cancelled, resulting in a small but finite deformation of Sc atom. On the other hand, the $4s$ electron in the other spin state (i.e., $\alpha 4s$) is deformed much less than $\beta 4s$ electron, and does not contribute so much to the screening. This is because the Coulomb repulsion, which is the key for the screening effect (see Sec. 4), is relevant between different spin states, while the Pauli principle makes the effects of the Coulomb repulsion between the same spins weaker.

Similar situations also occur in the other atoms presented in Table 1. For Ti atom (see also Table C8 in Appendix C), the large deformation is due to the $\alpha 3d_{yz}$ and the $\alpha 3d_{zx}$ orbitals, and in total the deformation is prolate ($\beta > 0$). The $\beta 4s$ orbital is deformed to cancel the

Table 1 Deformation parameters for the selected single-particle orbitals.

Atom	Orbital	$\beta_{\max}^{(\text{sp})}$
Al	$\alpha 3p_z$	0.6341
Sc	$\alpha 3p_z$	0.6341
Sc	$\alpha 3p_x$	0.6341
Sc	$\alpha 3d_{yz}$	-0.4530
Sc	$\alpha 4s$	-0.0098
Sc	$\beta 4s$	0.0830
Ti	$\alpha 3p_x$	0.6341
Ti	$\alpha 3p_z$	0.6341
Ti	$\alpha 3d_{zx}$	-0.4530
Ti	$\alpha 4s$	-0.0063
Ti	$\beta 4s$	-0.0530
Ni	$\alpha 3p_z$	0.6341
Ni	$\alpha 3d_{x^2-y^2}$	-0.4530
Ni	$\alpha 3d_{xy}$	-0.4530
Ni	$\alpha 3d_{yz}$	-0.4530
Ni	$\alpha 3d_{z^2}$	0.4388
Ni	$\alpha 4s$	-0.0163
Ga	$\alpha 3p_x$	0.6341
Ga	$\alpha 3p_z$	0.6341
Ga	$\alpha 3d_{x^2-y^2}$	-0.4530
Ga	$\alpha 3d_{yz}$	-0.4530
Ga	$\alpha 3d_{z^2}$	0.4576
Ga	$\alpha 4s$	-0.0008
Ga	$\alpha 4p_z$	0.6341

deformation of the $\alpha 3d$ orbitals. The $\alpha 4s$ orbital is also deformed but because the effects of the Coulomb repulsion is weakened by the Pauli principle, the deformation is much smaller. For Ni atom (Table C9 in Appendix C), the large prolate deformation created by the $\beta 3d_{z^2}$ orbital is slightly cancelled by the $\alpha 4s$ electron ³.

In the case of Ga atom (see also Table C10 in Appendix C), the large prolate deformation is due to the $\alpha 4p_z$ orbital $q_z^{(\text{sp})} = 11.1659 > 0$. With the same argument, we might expect that the $\beta 4s$ orbital should be largely deformed and cancel that of the $\alpha 4p_z$ orbital. However, the $\beta 4s$ orbital has rather small quadrupole moment $q_z^{(\text{sp})} = 0.0139$. It, therefore, does not cancel the deformation of the $\alpha 4p_z$ orbital, resulting in $Q_z = 11.1576$ of Ga atom as a whole. This is because $\langle r^2 \rangle$ of the $4s$ orbital is much smaller than that of the $\alpha 4p_z$ orbital, and

³ Since the eigenenergies of $d_{x^2-y^2}$ and d_{z^2} are identical if the system is completely spherical, the state with the last outer-most electron occupying $d_{x^2-y^2}$ is almost degenerate with the state with d_{z^2} . The deformation parameters β of these two states may have opposite sign, since $\beta^{(\text{sp})}$ of $d_{x^2-y^2}$ and d_{z^2} orbitals have the same absolute value but with the opposite sign (see Eqs. (2.23b) and (2.23c)). Therefore, there exist two states close in energy to each other which have opposite sign of β with almost the same absolute value.

thus the wave function of the $4s$ orbital does not have enough overlap region with the $\alpha 4p_z$ orbital to cancel its deformation.

We can also see the importance of the radii by comparing Sc, Ti, and Ni data in Tables 2, C8, and C9, respectively. For Sc atom, the quadrupole moment of the valence d electron is almost perfectly cancelled. On the other hand, it is marginally cancelled for Ti atom, while it is slightly cancelled for Ni atom. This behavior can be easily understood by noting that radius of the valence d orbital gets smaller as the atomic number increases: $\langle r^2 \rangle = 3.8, 2.9,$ and 1.5 Bohr^2 for Sc, Ti, and Ni atoms, respectively. The overlap between the valence d orbital and the $4s$ orbital gets smaller, which explains why the screening effects gets weaker as the atomic number increases in these atoms.

Moreover, the deformation of the d -block atoms becomes further smaller due to the radius of the valence single-particle orbitals, compared to that of the p -block atoms. The order of $\sum_m \langle r^2 \rangle_{n1} = 3 \langle r^2 \rangle_{n1}$ for the valence p orbital is the same as that of $Z \langle r^2 \rangle$ for the whole atom and thus $|\beta|$ of the p -block open-shell atoms are large, whereas the order of $\sum_m \langle r^2 \rangle_{n2} = 5 \langle r^2 \rangle_{n2}$ for the valence d orbital is smaller than that of $Z \langle r^2 \rangle$, since the s orbital with the principal quantum number $n + 1$ is, in general, also occupied.

Systematic behavior of β —With all these physical arguments, we can now fully understand the results in Fig. 3: We have found there that the p -block and d -block atoms can be deformed, but the deformation is much smaller for the d -block atoms compared with the p -block atoms showing single-particle-like deformation. This result can be explained by noting that the screening effects of the outer-most s orbital are rather significant for the d -block atoms, as discussed above for Sc, Ti, and Ni atoms. On the other hand, the outer-most valence p orbital of the p -block atom has much smaller overlap with the outer-most s orbital, so that the deformation caused by the valence p orbital remains unscreened.

This difference can also be understood by using deformation of the effective potential. As discussed in the beginning of this subsection, the effective potential remains almost spherical, while in the tail region it becomes anisotropic mainly due to the outer-most p or d orbitals. Consequently, such deformation can affect the orbitals which have larger spatial distribution. On the one hand, the outer-most s orbital of the d -block atoms, which has comparable $\langle r^2 \rangle$ to the valence orbital, is thus significantly affected by the anisotropic effective potential created by the valence d electrons. Accordingly, the s orbital can be deformed largely. On the other hand, the outer-most s orbital of the p -block atoms has smaller $\langle r^2 \rangle$ than the outer-most p orbital. Thus, the s orbital cannot be affected by such deformation of the effective potential, and, as a result, deformed largely.

Since deformation of the p -block atoms originates from single-particle-like deformation, atoms whose configurations of valence electrons are p^1 and p^4 always show prolate ($\beta > 0$) deformation and the last electron occupies p_z orbital. In contrast, atoms whose configurations of valence electrons are p^2 and p^5 always show oblate ($\beta < 0$) deformation and the last two electrons occupy p_x and p_y orbital. Since deformation of the d -block atoms induces the screening as discussed above, the deformation is small and the tendency is rather complicated.

Table 2 Mean-square radius $\langle r^2 \rangle_{nl}$, single-particle quadrupole moment $q_z^{(\text{sp})}$, and deformation parameter $\beta_z^{(\text{sp})}$ for single-particle orbitals of Sc atom calculated by the unrestricted Hartree-Fock method with 6-31+G basis. The single-particle energy of each orbital ε_j and corresponding orbital are also shown.

Spin	Orbital	ε_j	$\langle r^2 \rangle_{nl}$	$q_z^{(\text{sp})}$	$\beta_z^{(\text{sp})}$
α	1s	-165.8952	0.0073	0.0000	0.0000
α	2s	-19.0956	0.1393	0.0000	0.0000
α	2p _z	-15.6861	0.1162	0.0930	0.6341
α	2p _x	-15.6830	0.1164	-0.0466	-0.3171
α	2p _y	-15.6830	0.1164	-0.0466	-0.3171
α	3s	-2.5988	1.3396	-0.0031	-0.0018
α	3p _x	-1.6232	1.6265	-0.6506	-0.3171
α	3p _y	-1.6232	1.6265	-0.6506	-0.3171
α	3p _z	-1.5893	1.6107	1.2886	0.6341
α	3d _{xy}	-0.3375	3.7873	-2.1642	-0.4530
α	4s	-0.2171	17.4198	-0.2152	-0.0098
β	1s	-165.8951	0.0073	0.0000	0.0000
β	2s	-19.0832	0.1391	0.0001	0.0007
β	2p _z	-15.6837	0.1162	0.0929	0.6341
β	2p _x	-15.6657	0.1161	-0.0464	-0.3171
β	2p _y	-15.6657	0.1161	-0.0464	-0.3171
β	3s	-2.5451	1.3370	0.0387	0.0230
β	3p _z	-1.5798	1.6156	1.2925	0.6341
β	3p _x	-1.5273	1.6196	-0.6478	-0.3171
β	3p _y	-1.5273	1.6196	-0.6478	-0.3171
β	4s	-0.2051	18.5388	1.9406	0.0830
Total			53.1312	-0.4189	

3.5. Short conclusion

Before going to the qualitative discussion which will augment our results in this section by a qualitative model, let us summarize the results of the numerical calculations and the discussions in this section.

Firstly, as shown in Fig. 3 the closed-shell and half-closed-shell atoms are exactly spherical. The density distribution of the core electrons are spherical since it is the same as the noble-gas electronic configuration. Thus, the deformation comes from open-shell valence electrons. Since the valence orbital of the *s*-block atoms are also exactly spherical, only the *p*- or *d*-block atoms can be deformed, in principle. We find numerically that the deformation of the *p*-block atom is as large in order of magnitude as that of a single *p*-orbital deformation, while *d*-block atoms are much less deformed. The extremely tiny deformation of the *d*-block atoms are explained by the screening effect, where the outer-most *s* electrons are deformed to cancel the deformations of the inner *d* valence electrons, and the radii of the valence

electrons. The p -block atom is almost intact by the screening effect since the radius of the p -orbital is larger than that of s electrons.

Therefore, the deformations of the electron density in atoms at most originate from the single-particle orbitals of a few valence electrons, and there is no collective deformation. Rather, many-body effects in atoms disfavor deformations. With such tiny deformations, the effective potential is slightly deformed only in the surface and the tail (i.e., the valence electron) regions, but the dominant part remains spherical. This justifies the use of spherically symmetric effective potentials or density functionals in the conventional atomic structure calculations [25, 30, 77].

This is in stark contrast with nuclear systems. It is well known that nuclei can be deformed significantly via collective many-body effects, and they often have $|\beta| \gtrsim 0.3$ [5, 78]. In Appendix A, we exemplify this with model calculations for nuclear many-body systems. In the following section, we attempt to explain with a simple qualitative model why there is no collective deformation in the atoms whereas it exists in atomic nuclei.

4. Qualitative discussion

In the previous section and in Appendix A, we have shown that electrons in atoms are much less likely to deform than nucleons in atomic nuclei. We argue in this section that this difference physically originates from the nature of the inter-particle interactions: the repulsive Coulomb interaction between the electrons and the attractive nuclear force between the nucleons. To illustrate this point, we closely follow Refs. [79, 80]. We consider a system with N particles where the total-spin component, denoted as S_z , is conserved; $[\hat{H}, S_z] = 0$. By taking the N -body wave function as a simultaneous eigenstate of S_z and \hat{H} , the number of particles in each spin state is conserved, and we can regard the system as composed of N_\uparrow spin-up and N_\downarrow spin-down particles ($N = N_\uparrow + N_\downarrow$). We consider deforming spherical wave functions $\Psi_{\text{sph}}(\mathbf{r}_1, \dots, \mathbf{r}_N)$ with the following coordinate transformation:

$$\begin{aligned} & \Psi_{\text{def}}(x_1, y_1, z_1, \dots, x_N, y_N, z_N) \\ &= e^{N_\uparrow(2\beta_\uparrow - \alpha_\uparrow)/2} e^{N_\downarrow(2\beta_\downarrow - \alpha_\downarrow)/2} \Psi_{\text{sph}}(X_1, Y_1, Z_1, \dots, X_N, Y_N, Z_N), \end{aligned} \quad (4.1)$$

where $X_j = e^{\beta_\uparrow} x_j$, $Y_j = e^{\beta_\uparrow} y_j$, and $Z_j = e^{-\alpha_\uparrow} z_j$ for $j = 1, 2, \dots, N_\uparrow$ and $X_j = e^{\beta_\downarrow} x_j$, $Y_j = e^{\beta_\downarrow} y_j$, and $Z_j = e^{-\alpha_\downarrow} z_j$ for $j = N_\uparrow + 1, N_\uparrow + 2, \dots, N$. The coefficient $e^{N_a(2\beta_a - \alpha_a)/2}$ ($a = \uparrow, \downarrow$) is due to the normalization, which appears since, in the $\alpha_a \neq 2\beta_a$ case, the volume of the system is not conserved. Correspondingly, the single-particle densities of up- and down-spin states are also deformed as follows:

$$\rho_{\text{def}, \uparrow}(x, y, z) = e^{2\beta_\uparrow - \alpha_\uparrow} \rho_{\text{sph}, \uparrow}(e^{\beta_\uparrow} x, e^{\beta_\uparrow} y, e^{-\alpha_\uparrow} z), \quad (4.2a)$$

$$\rho_{\text{def}, \downarrow}(x, y, z) = e^{2\beta_\downarrow - \alpha_\downarrow} \rho_{\text{sph}, \downarrow}(e^{\beta_\downarrow} x, e^{\beta_\downarrow} y, e^{-\alpha_\downarrow} z). \quad (4.2b)$$

The coefficient $e^{2\beta_a - \alpha_a}$ also originates from the normalization coefficient in Eq. (4.1), or equivalently, the particle-number conservation;

$$\int \rho_{\text{def}, a}(\mathbf{r}) d\mathbf{r} = \int \rho_{\text{sph}, a}(\mathbf{r}) d\mathbf{r} = N_a. \quad (4.3)$$

Due to the saturation property, the atomic nuclei are expected to be deformed with the constant volume. For such deformation, $\alpha_a = 2\beta_a$ holds. Furthermore, as seen in Sec. 3,

atoms are also deformed with $\alpha = 2\beta$. Hence, in the following discussion, we will show the calculation with $\alpha_a = 2\beta_a$, and results with $\alpha_a \neq 2\beta_a$ will be shown in Appendix B, where we will reach essentially the same conclusion as those shown in this section. Note that $\alpha_a = 2\beta_a$ corresponds to the quadrupole deformation: It makes the wave function shrunken in the x - and y -axes, and elongated in the z -axis directions when β_a is positive. The quadrupole deformation of a spherical state $|\Psi_{\text{sph}}\rangle$ of the Hamiltonian $\hat{H} = \hat{T} + V_{\text{ext}} + V_{\text{int}}$, consisting of the kinetic energy operator \hat{T} , central external potential V_{ext} , and the interaction V_{int} , can be equivalently performed with the following canonical transformation:

$$|\Psi_{\text{def}}\rangle = e^{\beta_{\uparrow}[\hat{H}, \hat{Q}_{\uparrow}]} e^{\beta_{\downarrow}[\hat{H}, \hat{Q}_{\downarrow}]} |\Psi_{\text{sph}}\rangle. \quad (4.4)$$

Here, \hat{Q}_a is the quadrupole operator for each spin state defined as

$$\hat{Q}_{\uparrow} = m \sum_{j=1}^{N_{\uparrow}} \left[z_j^2 - \frac{1}{2} (x_j^2 + y_j^2) \right], \quad (4.5)$$

$$\hat{Q}_{\downarrow} = m \sum_{j=N_{\uparrow}+1}^N \left[z_j^2 - \frac{1}{2} (x_j^2 + y_j^2) \right], \quad (4.6)$$

where m and x_j, y_j, z_j are the mass and coordinates of the particles.

When the absolute value of the deformation parameter $|\beta_a|$ is small, the one-body density $\rho_{\text{def},a}$ of the system is written as follows:

$$\begin{aligned} \rho_{\text{def},a}(x, y, z) &= \rho_{\text{sph},a} \left(e^{\beta_a} x, e^{\beta_a} y, e^{-2\beta_a} z \right) \\ &= \rho_{\text{sph},a}(r) + f_a^{(1)}(\mathbf{r}) \frac{d\rho_{\text{sph},a}(r)}{dr} + f_a^{(2)}(\mathbf{r}) \frac{d^2\rho_{\text{sph},a}(r)}{dr^2} + O(\beta^3), \quad (4.7) \\ f_a^{(1)}(\mathbf{r}) &= \beta_a \frac{x^2 + y^2 - 2z^2}{r} + \beta_a^2 \frac{x^2 + y^2 + 4z^2}{r} \\ &\quad - \frac{\beta_a^2}{2} \frac{x^4 + y^4 + 4z^4}{r^3} + \beta_a^2 \frac{2(x^2 + y^2)z^2 - x^2y^2}{r^3} \\ &= -\sqrt{\frac{16\pi}{5}} \beta_a r Y_{20}(\theta, \phi) + \beta_a^2 \left[2r + \sqrt{\frac{16\pi}{5}} r Y_{20}(\theta, \phi) \right] - \frac{8\pi}{5} \beta_a^2 r [Y_{20}(\theta, \phi)]^2 \end{aligned} \quad (4.8)$$

$$\begin{aligned} f_a^{(2)}(\mathbf{r}) &= \frac{\beta_a^2}{2} \frac{x^4 + y^4 + 4z^4}{r^2} - \beta_a^2 \frac{2(x^2 + y^2)z^2 - x^2y^2}{r^2} \\ &= \frac{8\pi}{5} \beta_a^2 r^2 [Y_{20}(\theta, \phi)]^2. \end{aligned} \quad (4.9)$$

Let us consider how the energy of the system changes when we induce an infinitesimal quadrupole deformation $|\beta_a| \ll 1$ with this transformation to a spherically symmetric system $\rho_{\text{sph}}(\mathbf{r}) = \rho_{\text{sph}}(r)$.

Kinetic energy—The kinetic energy reads

$$\begin{aligned} T_{\text{def},a} &= \langle \Psi_{\text{def},a} | \hat{T} | \Psi_{\text{def},a} \rangle \\ &= \left(\frac{2}{3} e^{2\beta_a} + \frac{1}{3} e^{-4\beta_a} \right) \langle \Psi_{\text{sph},a} | \hat{T} | \Psi_{\text{sph},a} \rangle \\ &= \left(\frac{2}{3} e^{2\beta_a} + \frac{1}{3} e^{-4\beta_a} \right) T_{\text{sph},a} \end{aligned} \quad (4.10)$$

One can therefore see that the kinetic energy increases with the deformation

$$\Delta T_a := T_{\text{def},a} - T_{\text{sph},a} \simeq 4\beta_a^2 T_{\text{sph},a} > 0. \quad (4.11)$$

We also note that the deformation of a spin component does not affect the kinetic energy of the other spin component.

Central external potential energy—The central external potential energy of a system with density ρ is, in general, written as

$$E_{\text{ext}} = \int \rho(\mathbf{r}) V_{\text{ext}}(r) d\mathbf{r}. \quad (4.12)$$

Therefore, by using Eq. (4.7), the central external potential changes as

$$\begin{aligned} & \Delta E_{\text{ext},a} \\ & := E_{\text{ext},a}^{\text{def}} - E_{\text{ext},a}^{\text{sph}} \\ & = \int [\rho_{\text{def},a}(\mathbf{r}) - \rho_{\text{sph},a}(r)] V_{\text{ext}}(r) d\mathbf{r} \\ & \simeq \int f_a^{(1)}(\mathbf{r}) \frac{d\rho_{\text{sph},a}(r)}{dr} V_{\text{ext}}(r) d\mathbf{r} + \int f_a^{(2)}(\mathbf{r}) \frac{d^2\rho_{\text{sph},a}(r)}{dr^2} V_{\text{ext}}(r) d\mathbf{r} \\ & = \frac{32\pi}{5} \beta_a^2 \int_0^\infty \frac{d\rho_{\text{sph},a}(r)}{dr} V_{\text{ext}}(r) r^3 dr + \frac{8\pi}{5} \beta_a^2 \int_0^\infty \frac{d^2\rho_{\text{sph},a}(r)}{dr^2} V_{\text{ext}}(r) r^4 dr \\ & = -\frac{32\pi}{5} \beta_a^2 \int_0^\infty \rho_{\text{sph},a}(r) \frac{d}{dr} [V_{\text{ext}}(r) r^3] dr + \frac{8\pi}{5} \beta_a^2 \int_0^\infty \rho_{\text{sph},a}(r) \frac{d^2}{dr^2} [V_{\text{ext}}(r) r^4] dr, \end{aligned} \quad (4.13)$$

where we have assumed $V_{\text{ext}}(r) \sim r^d$ ($d > -3$) at $r \rightarrow 0$ in performing the partial integral in the final line.

Let us consider in particular the power-law type of external potential $V_{\text{ext}}(r) = cr^d$ with given constants c and d . Substituting this form into Eq. (4.13), one obtains

$$\Delta E_{\text{ext},a} \simeq \left[-\frac{8}{5}(d+3) + \frac{2}{5}(d+4)(d+3) \right] \beta_a^2 E_{\text{ext},a}^{\text{sph}} \quad (4.14)$$

In the case of the Coulomb potential ($d = -1$), Eq. (4.14) reads

$$\Delta E_{\text{ext},a} \simeq -\frac{4}{5} \beta_a^2 E_{\text{ext},a}^{\text{sph}} > 0. \quad (4.15)$$

In the case of the harmonic oscillator potential ($d = 2$), Eq. (4.14) reads

$$\Delta E_{\text{ext},a} \simeq 4\beta_a^2 E_{\text{ext},a}^{\text{sph}} > 0. \quad (4.16)$$

One can therefore see that the external potential energy increases with the deformation for both the Coulomb and harmonic oscillator potentials. As will be discussed later, they represent the Coulomb potential created by the atomic nucleus in atomic systems, and an external harmonic trap for a neutron drop discussed in Appendix A, respectively. We also note that the deformation of a spin component does not affect the potential energy of the other spin component.

Interaction energy—The interaction part of the energy, on the other hand, can either decrease or increase, and hence, favor or disfavor deformation depending on the nature of

the interaction. Also, as we shall show, the spins play an important role. To see this point, let us consider the direct (Hartree) part of the two-body interaction energy between the a and b spin states characterized by one-body density $\rho_{\text{def},a}(\mathbf{r})$:

$$E_{\text{int},ab}^{\text{def}} = \frac{1}{2} \iint V_{\text{int}}^{ab}(|\mathbf{r} - \mathbf{r}'|) \rho_{\text{def},a}(\mathbf{r}) \rho_{\text{def},b}(\mathbf{r}') d\mathbf{r} d\mathbf{r}', \quad (4.17)$$

where V_{int}^{ab} is the interaction between a particle with spin a and that with spin b . The total interaction energy, as long as we only consider the direct part, can then be written as $E_{\text{int,tot}}^{\text{def}} = E_{\text{int},\uparrow\uparrow}^{\text{def}} + 2E_{\text{int},\uparrow\downarrow}^{\text{def}} + E_{\text{int},\downarrow\downarrow}^{\text{def}}$. Notice that the multipole expansion of the interaction reads

$$V_{\text{int}}^{ab}(|\mathbf{r} - \mathbf{r}'|) = \sum_{l,m} V_l^{ab}(r, r') Y_{lm}(\theta, \phi) Y_{lm}^*(\theta', \phi'). \quad (4.18)$$

Substituting Eqs. (4.7) and (4.18) into Eq. (4.17), one obtains the change of the interaction energy induced by the deformation $\Delta E_{\text{int},ab} := E_{\text{int},ab}^{\text{def}} - E_{\text{int},ab}^{\text{sph}}$ as

$$\Delta E_{\text{int},ab} = \beta_a^2 \Delta \varepsilon_{\text{int},ab}^{(1)} + \beta_b^2 \Delta \varepsilon_{\text{int},ab}^{(2)} + \beta_a \beta_b \Delta \varepsilon_{\text{int},ab}^{(3)} + O(\beta^3), \quad (4.19)$$

with

$$\begin{aligned} \Delta \varepsilon_{\text{int},ab}^{(1)} &= \frac{16\pi}{5} \int_0^\infty \int_0^\infty \frac{d\rho_{\text{sph},a}(r)}{dr} \rho_{\text{sph},b}(r') V_0^{ab}(r, r') r^3 r'^2 dr dr' \\ &\quad + \frac{4\pi}{5} \int_0^\infty \int_0^\infty \frac{d^2 \rho_{\text{sph},a}(r)}{dr^2} \rho_{\text{sph},b}(r') V_0^{ab}(r, r') r^4 r'^2 dr dr', \end{aligned} \quad (4.20a)$$

$$\begin{aligned} \Delta \varepsilon_{\text{int},ab}^{(2)} &= \frac{16\pi}{5} \int_0^\infty \int_0^\infty \rho_{\text{sph},a}(r) \frac{d\rho_{\text{sph},b}(r')}{dr'} V_0^{ab}(r, r') r^2 r'^3 dr dr' \\ &\quad + \frac{4\pi}{5} \int_0^\infty \int_0^\infty \rho_{\text{sph},a}(r) \frac{d^2 \rho_{\text{sph},b}(r')}{dr'^2} V_0^{ab}(r, r') r^2 r'^4 dr dr' = \Delta \varepsilon_{\text{int},ba}^{(1)}, \end{aligned} \quad (4.20b)$$

$$\Delta \varepsilon_{\text{int},ab}^{(3)} = \frac{8\pi}{5} \int_0^\infty \int_0^\infty \frac{d\rho_{\text{sph},a}(r)}{dr} \frac{d\rho_{\text{sph},b}(r')}{dr'} V_2^{ab}(r, r') r^3 r'^3 dr dr'. \quad (4.20c)$$

To be more explicit, for the parallel spin states, one finds

$$\Delta E_{\text{int},aa} = \beta_a^2 \left(\Delta \varepsilon_{\text{int},aa}^{(1)} + \Delta \varepsilon_{\text{int},aa}^{(2)} + \Delta \varepsilon_{\text{int},aa}^{(3)} \right) + O(\beta^3) \quad (4.21)$$

and for the anti-parallel spin states ($a \neq b$)

$$\Delta E_{\text{int},ab} = \beta_\uparrow^2 \Delta \varepsilon_{\text{int},ab}^{(1)} + \beta_\downarrow^2 \Delta \varepsilon_{\text{int},ab}^{(2)} + \beta_\uparrow \beta_\downarrow \Delta \varepsilon_{\text{int},ab}^{(3)} + O(\beta^3). \quad (4.22)$$

First, let us consider the case of atomic nuclei. We note that the interaction between nucleons in vacuum are not yet rigorously known, but it basically comprises of relatively long-range attractive forces originating from exchanges of several mesons and a short-range repulsive force [81–85]. These combined together have a net attractive effect between nucleons, which results in a bound state of a proton and a neutron (i.e., deuteron) [86, 87], and in a large negative scattering length between nucleons [83, 84]. We also note that an effective in-medium nucleon-nucleon interaction used in nuclear many-body calculations in general has a net attractive effect [88]. For our qualitative discussion in this section, a simple delta-function force $V_{\text{int}}^{ab}(\mathbf{r}) = -g_{ab} \delta(\mathbf{r})$ suffices to model this net nuclear force between the nucleons. The parameter g_{ab} is positive when the interaction is attractive, such as for nuclear

systems, whereas it is negative when the interaction is repulsive. The multipole expansion of this potential reads

$$V_0^{ab}(r, r') = V_2^{ab}(r, r') = -g_{ab} \frac{\delta(r - r')}{rr'}. \quad (4.23)$$

Substituting Eq. (4.23) into Eqs. (4.19) and (4.20), one obtains

$$\begin{aligned} & \Delta E_{\text{int}, ab} \\ \simeq & -\frac{16\pi g_{ab}}{5} \beta_a^2 \int_0^\infty \frac{d\rho_{\text{sph}, a}(r)}{dr} \rho_{\text{sph}, b}(r) r^3 dr - \frac{4\pi g_{ab}}{5} \beta_a^2 \int_0^\infty \frac{d^2 \rho_{\text{sph}, a}(r)}{dr^2} \rho_{\text{sph}, b}(r) r^4 dr \\ & -\frac{16\pi g_{ab}}{5} \beta_b^2 \int_0^\infty \rho_{\text{sph}, a}(r) \frac{d\rho_{\text{sph}, b}(r)}{dr} r^3 dr - \frac{4\pi g_{ab}}{5} \beta_b^2 \int_0^\infty \rho_{\text{sph}, a}(r) \frac{d^2 \rho_{\text{sph}, b}(r)}{dr^2} r^4 dr \\ & -\frac{8\pi g_{ab}}{5} \beta_a \beta_b \int_0^\infty \frac{d\rho_{\text{sph}, a}(r)}{dr} \frac{d\rho_{\text{sph}, b}(r)}{dr} r^4 dr \\ = & \frac{4\pi g_{ab}}{5} (\beta_a - \beta_b)^2 \int_0^\infty \frac{d\rho_{\text{sph}, a}(r)}{dr} \frac{d\rho_{\text{sph}, b}(r)}{dr} r^4 dr. \end{aligned} \quad (4.24)$$

Thus, on the one hand, the interaction energy for the same spin component does not change with the deformation: $\Delta E_{\text{int}, \uparrow\uparrow} = \Delta E_{\text{int}, \downarrow\downarrow} = 0$. This can be also shown using Eq. (4.17) without using the multipole expansion. This is due to a scaling symmetry of the delta function interaction. On the other hand, the interaction energy of the anti-parallel spin states $E_{\text{int}, \uparrow\downarrow}^{\text{def}}$ can be non-zero. Indeed, in the nuclear system, the one-body density is more or less constant in the interior region due to its saturation property, $d\rho_{\text{sph}}/dr \simeq 0$, and it suddenly decreases at the surface region $d\rho_{\text{sph}}/dr < 0$. Thus, it is reasonable to assume $d\rho_{\text{sph}}/dr \leq 0$ in the most region. Therefore, for the anti-parallel spin states $a \neq b$, the integral of Eq. (4.24) is positive. For the attractive interaction $g_{\uparrow\downarrow} > 0$, it is energetically favorable to have $\beta_a = \beta_b$, so that there is no energy increase with the deformation, i.e., $\Delta E_{\text{int}, \uparrow\downarrow} \simeq 0$. Hence, the spin-up and -down particles deform in the same manner, i.e., $\rho_{\text{def}, \uparrow}(\mathbf{r}) = \rho_{\text{def}, \downarrow}(\mathbf{r})$. We note that we have assumed in the above argument the simplest delta-function interaction. In reality, the modern nuclear effective interaction, such as the Skyrme interaction, contains the terms simulating finite-range effects (e.g., t_1 and t_2 terms in Eq. (A2)). This finite-range effects can make the energy of the system decrease with the nuclear deformation, in contrast to what have been found above with a delta interaction. The above argument can thus only explain why the condition $\beta_a = \beta_b$ is favored: Once the nuclear deformation occurs with the finite-range effects or other reasons, the nuclei deform in a spin-independent manner due to the attractive nature of interaction.

In contrast, if the interaction was repulsive $g_{\uparrow\downarrow} < 0$, the energy can decrease with the deformation $\Delta E_{\text{int}, \uparrow\downarrow} < 0$. In particular, the condition $\beta_a = -\beta_b$ is favored, so that the spin-up and spin-down particles undergo the opposite quadrupole deformation. They cancel with each other when one considers the total density $\rho_{\text{def}}(\mathbf{r}) = \rho_{\text{def}, \uparrow}(\mathbf{r}) + \rho_{\text{def}, \downarrow}(\mathbf{r})$, so that the net deformation of the whole system is suppressed.

Next, let us consider the case of atoms. The multipole expansion of the Coulomb interaction reads

$$V_l(r, r') = \frac{4\pi}{2l+1} \frac{r_{<}^l}{r_{>}^{l+1}}, \quad (4.25)$$

where $r_<$ and $r_>$ are smaller and greater ones of r and r' , respectively. Substituting Eq. (4.25) into Eqs. (4.20), one obtains

$$\begin{aligned}\Delta\varepsilon_{\text{int},ab}^{(1)} &= \frac{64\pi^2}{5} \int_0^\infty \int_0^\infty \frac{d\rho_{\text{sph},a}(r)}{dr} \rho_{\text{sph},b}(r') \frac{1}{r_>} r^3 r'^2 dr dr' \\ &\quad + \frac{16\pi^2}{5} \int_0^\infty \int_0^\infty \frac{d^2\rho_{\text{sph},a}(r)}{dr^2} \rho_{\text{sph},b}(r') \frac{1}{r_>} r^4 r'^2 dr dr' \\ &= \frac{16\pi^2}{5} \int_0^\infty \int_0^\infty \theta(r-r') \frac{d\rho_{\text{sph},a}(r)}{dr} \rho_{\text{sph},b}(r') r^2 r'^2 dr dr',\end{aligned}\quad (4.26a)$$

$$\begin{aligned}\Delta\varepsilon_{\text{int},ab}^{(3)} &= \frac{32\pi^2}{25} \int_0^\infty \int_0^\infty \frac{d\rho_{\text{sph},a}(r)}{dr} \frac{d\rho_{\text{sph},b}(r')}{dr'} \frac{r^2}{r_>} r^3 r'^3 dr dr' \\ &= \frac{32\pi^2}{25} \int_0^\infty \int_0^\infty \frac{d\rho_{\text{sph},a}(r)}{dr} \frac{d\rho_{\text{sph},b}(r')}{dr'} [\theta(r-r') r'^5 + \theta(r'-r) r^5] dr dr',\end{aligned}\quad (4.26b)$$

where $\theta(r)$ is the Heaviside step function defined by

$$\theta(r) = \begin{cases} 0 & (r < 0), \\ 1 & (r > 0). \end{cases}\quad (4.27)$$

In the atomic system, the one-body density ρ_{sph} is generally a decreasing function of r , except for the surface region (which will be discussed in this section), so that it is reasonable to assume $d\rho_{\text{sph}}/dr \leq 0$ in the most region. Hence, one can find $\Delta\varepsilon_{\text{int},ab}^{(1)} = \Delta\varepsilon_{\text{int},ba}^{(2)} < 0$ and $\Delta\varepsilon_{\text{int},ab}^{(3)} > 0$. One can also see for the parallel spin states

$$\begin{aligned}\Delta\varepsilon_{\text{int},aa}^{(1)} + \Delta\varepsilon_{\text{int},aa}^{(2)} + \Delta\varepsilon_{\text{int},aa}^{(3)} \\ = \frac{32\pi^2}{5} \int_0^\infty \int_0^\infty \theta(r-r') \frac{d\rho_{\text{sph},a}(r)}{dr} \rho_{\text{sph},a}(r') (r^2 - r'^2) r'^2 dr dr' < 0.\end{aligned}\quad (4.28)$$

Therefore, when one considers the interaction energy between the parallel spin [Eq. (4.21)], one finds that the right-hand side of Eq. (4.21) is negative, and thus the Coulomb interaction favors deformation. This is a well-known fact in a nuclear fission problem, when the deformed Coulomb energy is evaluated with the liquid-drop model [5, 89]. In addition, if one considers the interaction between the different spin [Eq. (4.22)], deformation with the different sign $\beta_\uparrow = -\beta_\downarrow$ is energetically favored because of the positive $\Delta\varepsilon_{\text{int},\uparrow\downarrow}^{(3)}$. The effect of $\Delta\varepsilon_{\text{int},\uparrow\downarrow}^{(1)}$ and $\Delta\varepsilon_{\text{int},\uparrow\downarrow}^{(2)}$ also favors deformation because $\Delta\varepsilon_{\text{int},\uparrow\downarrow}^{(1)} = \Delta\varepsilon_{\text{int},\downarrow\uparrow}^{(2)} < 0$. Therefore, the Coulomb repulsive interaction favors spin-dependent deformation: ρ_\uparrow and ρ_\downarrow makes the opposite quadrupole deformations. When one considers the deformation of the total density $\rho_{\text{def}}(\mathbf{r}) = \rho_{\text{def},\uparrow}(\mathbf{r}) + \rho_{\text{def},\downarrow}(\mathbf{r})$, they cancel with each other and the total deformation would be small. These conclusions are in line with those for the repulsive delta function interaction. However, in contrast to the delta function interaction, there exists non-vanishing contribution from the parallel spin states $\Delta E_{\text{int},aa}$.

Overall discussion—From these qualitative discussions, we can see that difference in the nature of the interaction is the key in understanding why atoms do not tend to deform collectively while nuclei do. The kinetic energy and the central external potential energy increase with the deformation, hence disfavor the deformation (see Eqs. (4.11), (4.15), and

(4.16)). The interaction energy, on the other hand, may decrease with the deformation depending on the nature of the interaction. In this connection, we mention that the well-known Hund rule [71–75] is also intimately related to the repulsive nature of electron-electron interaction, as has been argued in Ref. [90]. If this decrease is greater than the increase of the kinetic and external potential energies, the system would deform. One finds above that an attractive short-range interaction, modeled by the delta function interaction, favors deformation in a spin-independent manner $\beta_{\uparrow} = \beta_{\downarrow}$ (see Eq. (4.24)). The repulsive Coulomb interaction energy, on the other hand, favors spin-dependent deformation $\beta_{\uparrow} = -\beta_{\downarrow}$, in a manner to cancel with each other the deformation of the total density $\rho_{\text{def}}(\mathbf{r}) = \rho_{\text{def},\uparrow}(\mathbf{r}) + \rho_{\text{def},\downarrow}(\mathbf{r})$ (see Eq. (4.28) and its discussion below). The former represents nuclear systems, and the latter represents atomic systems. The above results thus qualitatively explain why nuclear systems can deform significantly while atomic systems cannot.

This model discussion is closely related to the screening effects of electrons numerically found and discussed in Sec. 3. The screening effect occurs due to the repulsive Coulomb interaction, which aims to decrease any charge imbalance. If, for example, the spin-up electrons make a positive quadrupole deformation, the down spins attempt to make a negative quadrupole deformation to attain the charge neutrality. Therefore, the above argument based on the multipole component of the interaction is consistent with the screening effect. Indeed, we have found in Sec. 3 that the deformation of the valence d -orbital is cancelled by the deformation of the opposite spin in the s -orbital for the d -block atoms. This is in line with the above model calculation. We have also found in Sec. 3 that the deformations of atoms occur only in the valence electron region for p - and d -block atoms. We can also explain this by using the above model: The central external potential energy, favoring spherical shape, is great in the central region. Therefore, even if the interaction energy is negative and favors deformation, it is difficult to overcome the positive potential energy. It is thus rather unlikely for the central region of the atoms to undergo significant deformations. In the valence electron region, on the other hand, the potential energy becomes small and it is easier for the interaction energy to overcome it. This qualitatively explains why atoms can be deformed only in the valence electron region.

As the above discussions for the quadrupole deformation may also apply to the higher order multipole deformations at any order, we can conjecture the following statement for general infinitesimal deformations: The multipole component of the inter-particle interaction must be attractive for the system to undergo significant collective deformations. The Coulomb interaction between the electrons has repulsive multipole components for all orders, and therefore the deformations of up-spin and down-spin states cancels with each other for all multipole orders, resulting in a small total deformation as numerically found in the previous section. The nuclear force, on the other hand, may undergo spin-independent deformations when a multipole component of the interaction is attractive and strong enough.

We note that we have assumed in the above model argument that $d\rho_{\text{sph}}/dr \leq 0$. While this assumption is valid for closed shell atoms and also for open-shell atoms in their central region, the electron density usually oscillates for open-shell atoms in the surface region: The electron density in the surface region is mostly determined by the wave function of the outermost valence electrons $\psi_{nlms}(r, \theta, \phi)$, which show oscillations with r when $n > 1$. Thus, the above model argument in the valence electron region should be taken with some cautions.

We also note that we have neglected in the above discussion the exchange-correlation part in evaluating the interaction energy [Eq. (4.17)]. In the Hartree-Fock theory and the density functional theory, the exchange or exchange-correlation part is generally found to be sub-dominant than the direct part contributions for electrons in atoms [30, 51, 77, 91]. We have, therefore, only considered the direct part in our basic qualitative discussions above, while one needs to include the exchange-correlation part for more elaborated descriptions. In particular, for electrons in the surface region of atoms (i.e., the valence orbital), the exchange-correlation part becomes more important compared with the central region, because the density is rather small and thus the electrons are strongly correlated [51, 77, 92]. Our model discussion on the surface region of atoms, therefore, should be at best qualitative one. In the nuclear DFT, on the other hand, the direct and exchange parts are usually not considered separately. Rather, a short-range attractive effective interaction $V_{\text{int}}(|\mathbf{r} - \mathbf{r}'|)$ in Eq. (4.17) is often used whose shape and parameters are chosen to reproduce well nuclear properties measured in experiments [88, 93, 94]. Thus, the above argument based on Eq. (4.17), ostensibly considering only the direct part of interaction energy, naturally contains many-body correlation effects, including those due to the three-body and tensor interaction, and therefore should be valid even though atomic nuclei are rather strongly correlated.

While we have shown that atoms in their ground states are unlikely to be deformed significantly, we may expect larger deformations in more exotic atomic systems. As can be seen in our qualitative discussion above, atoms may be deformed if the condition $d\rho_{\text{sph}}/dr \leq 0$ does not hold or if the exchange-correlation term dominates the direct term. These are often the cases for highly excited atoms. In particular, we can expect that Rydberg atoms [95–97], which have electrons in excited states with extremely large principal quantum numbers, may show significant deformations. While the Rydberg atoms with one electron excited to such orbital will trivially show a deformed shape representing the single-particle orbital, they may show non-trivial collective deformations when more than one electrons are excited in the Rydberg orbits [97].

5. Conclusion

We have investigated numerically whether the electron distribution of atoms can be deformed. To this end, we have calculated the deformation parameters for various atoms with a wide variety of different many-body methods, and have found that the noble-gas, half-shell-closed, and s -block atoms are spherical, while the p - and d -block atoms are deformed. The deformations of the p - and d -block atoms are neither collective nor significantly deformed. We have shown that the core part remains spherical even for these atoms, and their deformations originate from a few valence electrons. Therefore, the deformations of the atoms are at most of a single-particle nature of a few valence electrons: Atoms do not deform collectively, in contrast to nuclei. We have also shown that the many-body effects of electrons in atoms tend to make the deformations smaller due to the screening effect.

Owing to the deformation, the self-consistent effective mean-field potential for p - and d -block atoms is slightly deformed in the surface and the tail region. Therefore, the core electrons are still eigenstates of angular momentum and are described by single spherical harmonics, whereas the valence electrons are not. We have found numerically that the degeneracy of the valence electrons are indeed lifted due to this effect, but the effect is 0.05 Hartree

or much less. Hence, calculations of the atomic structure with spherical symmetry are still justified.

We have compared the atomic deformation to the nuclear deformation by using a qualitative model. We have argued that the difference between them originates from the properties of the inter-particle interactions. On the one hand, in the case of atomic nuclei, the interaction is of attractive in net, and the deformation of the spin-up component favors to be the same as that of the spin-down component. Consequently, the collective deformation can occur. On the other hand, in the case of atoms, the interaction is purely repulsive, and the deformation of the spin-up component favors to be the opposite of that of the spin-down component, cancelling each other. Accordingly, the collective deformation does not occur.

While the collective deformations of nuclei have clearly been observed by the gamma-ray spectroscopy of their rotational spectra of Eq. (2.1), the atomic deformations studied in this work are neither significant nor collective, and therefore should not show similar rotational spectra. One rather needs to directly probe the density distribution of the electrons to experimentally test the deformations found by our numerical calculations. It would be rather challenging but we expect that they may be directly observed with recent atomic and molecular physics technology, such as photo-ionization microscopy [98, 99], or tomographic imaging [100].

Acknowledgment

We thank Gianluca Colò, Yoshiko Kanada-En'yo, Haozhao Liang, Takashi Nakatsukasa, and Kenichi Yoshida for fruitful discussion. The RIKEN iTHEMS program, the JSPS Grant-in-Aid for JSPS Fellows under Grant No. JP19J20543, and JSPS KAKENHI Grant No. JP19K03861 are acknowledged. The numerical calculations were performed on cluster computers at the RIKEN iTHEMS program.

A. Deformation of neutron drop in a harmonic trap

In this Appendix, we discuss an illustrative case of deformed systems: that is, a neutron drop trapped in a spherical harmonic potential. Even though neutron drops are fictitious, they provide useful systems to benchmark many-body theories [101–108]. As the density can be controlled by changing the strength of the trapping potential. They have also been utilized in connection with neutron-rich nuclei and neutron stars [109]. By using this model, we show in this Appendix that, within HF theory, the nuclear systems are indeed collectively deformed due to the attractive nuclear force: The systems are collectively deformed when the inter-particle attraction is strong enough, while they do not if the interaction is repulsive.

Although the interaction between neutrons is attractive, in contrast to the interaction between electrons, typical nuclear interactions are not strong enough so that systems consisting solely of neutrons do not bound by themselves. To study properties of many-neutron systems, one thus needs to introduce an external confining potential, analogously to the electron-nucleus external potential in atoms. In this Appendix, we use an isotropic harmonic oscillator potential,

$$V_{\text{ext}}(r) = \frac{1}{2}m_n\Omega^2r^2, \quad (\text{A1})$$

where $m_n = 939.6 \text{ MeV}/c^2$ is the neutron mass [110], to localize the neutrons in neutron drops. In this study, we set $\hbar\Omega = 5 \text{ MeV}$.

To take into account the interaction between neutrons, we employ the HF theory with the Skyrme effective interaction [93, 94]. The Skyrme interaction is a zero-range force with momentum and density dependences, given by

$$\begin{aligned}
v_{\text{Sk}} = & t_0 (1 + x_0 P_\sigma) \delta(\mathbf{r}_1 - \mathbf{r}_2) - \frac{t_1}{8} (1 + x_1 P_\sigma) \left[\overleftarrow{\nabla}^2 \delta(\mathbf{r}_1 - \mathbf{r}_2) + \delta(\mathbf{r}_1 - \mathbf{r}_2) \overrightarrow{\nabla}^2 \right] \\
& + \frac{t_2}{4} (1 + x_2 P_\sigma) \left[\overleftarrow{\nabla} \delta(\mathbf{r}_1 - \mathbf{r}_2) \cdot \overrightarrow{\nabla} \right] + \frac{t_3}{6} (1 + x_3 P_\sigma) \delta(\mathbf{r}_1 - \mathbf{r}_2) \left\{ \rho \left(\frac{\mathbf{r}_1 + \mathbf{r}_2}{2} \right) \right\}^\alpha \\
& + i \frac{W_0}{4} \left[\overleftarrow{\nabla} \times \delta(\mathbf{r}_1 - \mathbf{r}_2) \overrightarrow{\nabla} \right] \cdot (\boldsymbol{\sigma}_1 + \boldsymbol{\sigma}_2), \tag{A2}
\end{aligned}$$

where $\overrightarrow{\nabla} = \nabla_1 - \nabla_2$ acting on the right and $\overleftarrow{\nabla} = \nabla_1 - \nabla_2$ acting on the left, and $P_\sigma = (1 + \boldsymbol{\sigma}_1 \cdot \boldsymbol{\sigma}_2)/2$ is the spin-exchange operator. The coefficients t_i , x_i ($i = 0-3$), α , and W_0 are the parameters to be adjusted to properties of the homogeneous nucleon gas, called nuclear matter, and experimentally observed nuclear properties. Among these, the t_0 and t_3 terms determine the bulk property of nuclei. The former is attractive, and the latter with density dependence ($\alpha > 0$) is repulsive. The repulsive t_3 term, which becomes dominant over the other terms at high densities, is responsible for the saturation of nuclear matter density.

In our study, we adopt the SkM* parameter set [111] given in Table A1. In order to see how the deformation property depends on the strength and the sign of the interaction, we scale the strength parameters of the Skyrme interaction as $t_i \rightarrow f t_i$ for $i = 0, 1, 2$ and $t_3 \rightarrow |f| t_3$ with f being varied within the range $[-1, 1]$, where $f = 1$ corresponds to the original. The t_3 term is kept repulsive to avoid collapse of the system. In our numerical calculations, reflection and axial symmetries are imposed.

Table A1 Values of t_0 (MeV fm³), t_1 (MeV fm⁵), t_2 (MeV fm⁵), t_3 (MeV fm^{3(1+ α)}), x_0 , x_1 , x_2 , x_3 , α , and W_0 (MeV fm⁵) of the SkM* parameter set [111].

t_0	t_1	t_2	t_3	x_0	x_1	x_2	x_3	α	W_0
-2645	410	-135	15595	0.09	0	0	0	1/6	130

To find HF solutions for a neutron drop, we perform several HF iterations for each system starting from prolate and oblate configurations. Most often, a prolate (oblate) initial condition ends up with a prolate (oblate) solution for open-shell systems. For closed-shell systems, on the other hand, a spherical solution is obtained regardless of the initial deformation if it is energetically favored.

Fig. A1 shows the deformation parameters of the neutron drops ^{8-40}n with attractive ($f > 0$) interactions. Here, $^N n$ denotes the system with N neutrons. The spherical solutions are shown by open circles. The prolate and oblate solutions are respectively plotted by solid and open symbols. Squares, diamonds, and triangles correspond to the solutions for $f = 1, 0.6$, and 0.2 , respectively. As can be seen from the figure, many of the neutron drops examined here have both prolate and oblate solutions, often at similar energies to each other. The quadrupole deformation tends to be smaller as the strengths of the attractive interaction decrease. This behavior of the deformation can be understood as follows: as the interaction is weakened, the effect of the spherical external field becomes more significant relative to the interaction, which is consistent with the discussion shown in Sec. 4. As a result, the system

tends to adjust its density distribution closer to the spherical shape to reduce the potential energy of the external field. The systems with $N = 8, 16, 20, 32, 34,$ and 40 are spherical for all the values of the scaling parameter f . They correspond to closed-shell configurations, *e.g.*, $(1s_{1/2})^2 (1p_{3/2})^4 (1p_{1/2})^2$ for 8n , $(1s_{1/2})^2 (1p_{3/2})^4 (1p_{1/2})^2 (1d_{5/2})^6 (2s_{1/2})^2$ for ^{16}n , and $(1s_{1/2})^2 (1p_{3/2})^4 (1p_{1/2})^2 (1d_{5/2})^6 (2s_{1/2})^2 (1d_{3/2})^4$ for ^{20}n .

We have also carried out HF calculations with repulsive ($f < 0$) interactions, but we obtained spherical solutions for only a few systems with closed-shell configurations, and no deformed solution was found. Although the pairing correlation would stabilize the convergence and allows us to study repulsive systems as well as the attractive ones, in this appendix we only consider systems with variable attractive interaction within the HF theory.

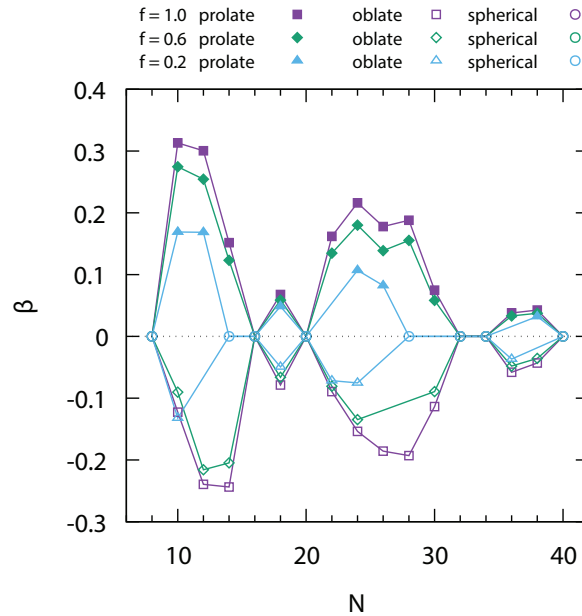


Fig. A1 Deformation parameters of HF solutions for the neutron drops ^{8-40}n with $\hbar\Omega = 5$ MeV. Here, f is the scaling factor of the strengths of Skyrme interaction (see the main text for details). When there are two solutions both on prolate and oblate sides, both are plotted in the figure.

In Figs. A2 and A3, we show the density distributions of prolate and oblate solutions, respectively, of ^{14}n for different values of f . In both cases, we see clearly that the density becomes tighter and more deformed as f changes from 0.2 to 1.

Evidently, neutrons trapped in an isotropic harmonic-oscillator potential can be collectively deformed for open-shell systems, in contrast to electrons in atoms, as is argued in Sec. 4. As expected, the spherically symmetric external field tends to suppress the deformation parameter as well as the radius of the system. This conclusion is consistent with the qualitative discussion in Sec. 4.

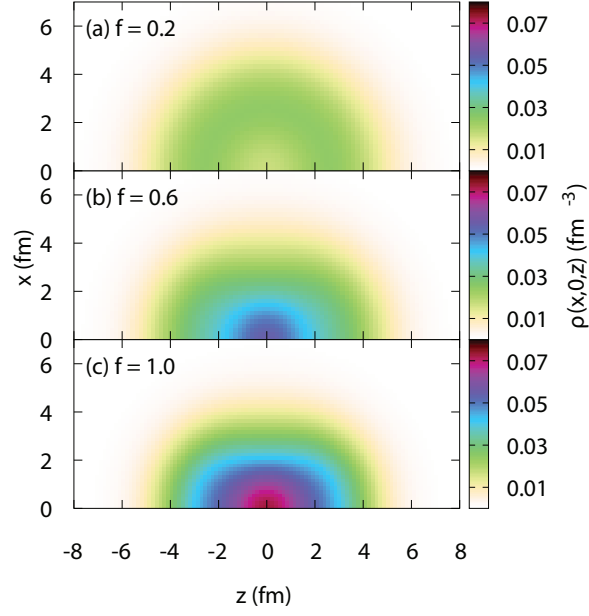


Fig. A2 Densities of the prolate HF solutions on x - z plane of ^{14}n for (a) $f = 0.2$, (b) $f = 0.6$, and (c) $f = 1.0$. The horizontal (z) axis is the axis of symmetry.

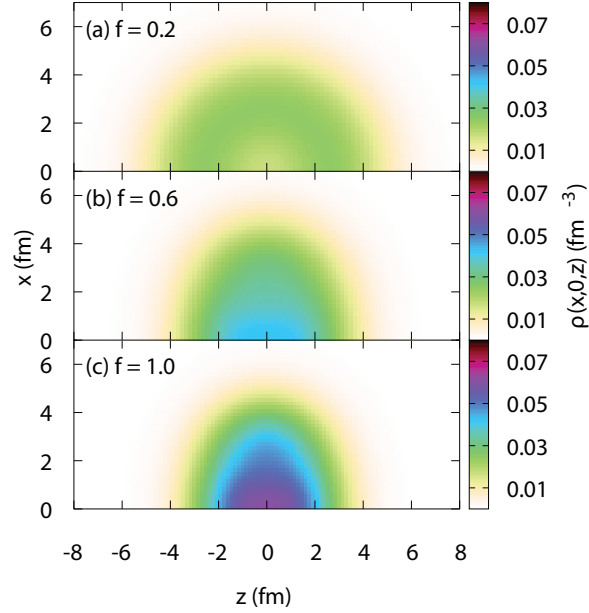


Fig. A3 Same as Fig. A2 but for the oblate HF solutions.

B. Generalization of Sec. 4

In this Appendix, we will show the general case (i.e., $\alpha_a \neq 2\beta_a$) of the calculations shown in Sec. 4. Firstly, the single-particle densities of up- and down-spin states are defined as follows:

$$\rho_{\text{def},a}(\mathbf{r}) = \frac{1}{2} \sum_{j=1}^N \int \Psi_{\text{def}}^*(\mathbf{r}_1, \dots, \mathbf{r}_N) (1 \pm \sigma_{zj}) \delta(\mathbf{r} - \mathbf{r}_j) \Psi_{\text{def}}(\mathbf{r}_1, \dots, \mathbf{r}_N) d\mathbf{r}_1 \dots d\mathbf{r}_N, \quad (\text{B1})$$

where $+$ in $1 \pm \sigma_{zj}$ for $a = \uparrow$ and $-$ for $a = \downarrow$. For simplicity, the spin coordinates of particles (\uparrow for particle $j = 1, 2, \dots, N_\uparrow$ and \downarrow for particle $j = N_\uparrow + 1, N_\uparrow + 2, \dots, N$) are omitted. Using the notation of \mathbf{R}_a , \mathbf{r} , \mathbf{R}_j , and \mathbf{r}_j which denote $\mathbf{R}_a = (e^{\beta_a} x, e^{\beta_a} y, e^{-\alpha_a} z)$, $\mathbf{r} = (x, y, z)$, $\mathbf{R}_j = (e^{\beta_j} x, e^{\beta_j} y, e^{-\alpha_j} z)$, $\mathbf{r}_j = (x_j, y_j, z_j)$, and the relation $\delta(\mathbf{r} - \mathbf{r}_j) = e^{-(\alpha_a - 2\beta_a)} \delta(\mathbf{R}_a - \mathbf{R}_j)$, one obtains

$$\begin{aligned}
& \rho_{\text{def}, a}(\mathbf{r}) \\
&= \frac{1}{2} \sum_{j=1}^N \int \Psi_{\text{sph}}^*(\mathbf{R}_1, \dots, \mathbf{R}_N) (1 \pm \sigma_{zj}) \delta(\mathbf{r} - \mathbf{r}_j) \Psi_{\text{sph}}(\mathbf{R}_1, \dots, \mathbf{R}_N) d\mathbf{R}_1 \dots d\mathbf{R}_N \\
&= \frac{1}{2} \sum_{j=1}^N e^{2\beta_a - \alpha_a} \int \Psi_{\text{sph}}^*(\mathbf{R}_1, \dots, \mathbf{R}_N) (1 \pm \sigma_{zj}) \delta(\mathbf{R}_a - \mathbf{R}_j) \Psi_{\text{sph}}(\mathbf{R}_1, \dots, \mathbf{R}_N) d\mathbf{R}_1 \dots d\mathbf{R}_N \\
&= e^{2\beta_a - \alpha_a} \rho_{\text{sph}, a}(\mathbf{R}_a). \tag{B2}
\end{aligned}$$

First of all, when the absolute value of the deformation parameters $|\alpha_a|$ and $|\beta_a|$ are small, the one-body density $\rho_{\text{def}, a}$ of the system reads

$$\begin{aligned}
\rho_{\text{def}, a}(x, y, z) &= \rho_{\text{sph}, a}(e^{\beta_a} x, e^{\beta_a} y, e^{-\alpha_a} z) \\
&= \left[1 + (2\beta_a - \alpha_a) + \frac{1}{2} (2\beta_a - \alpha_a)^2 \right] \rho_{\text{sph}, a}(r) \\
&\quad + f_a^{(1)}(\mathbf{r}) \frac{d\rho_{\text{sph}, a}(r)}{dr} + f_a^{(2)}(\mathbf{r}) \frac{d^2\rho_{\text{sph}, a}(r)}{dr^2} + O(\beta^3), \tag{B3}
\end{aligned}$$

$$\begin{aligned}
f_a^{(1)}(\mathbf{r}) &= [1 + (2\beta_a - \alpha_a)] \left(\beta_a \frac{x^2 + y^2}{r} - \alpha_a \frac{z^2}{r} \right) \\
&\quad + \beta_a^2 \frac{x^2 + y^2}{r} + \alpha_a^2 \frac{z^2}{r} - \frac{\beta_a^2}{2} \frac{x^4 + y^4}{r^3} - \frac{\alpha_a^2}{2} \frac{z^4}{r} - \beta_a^2 \frac{x^2 y^2}{r^3} + \alpha_a \beta_a \frac{(x^2 + y^2) z^2}{r^3}, \tag{B4}
\end{aligned}$$

$$f_a^{(2)}(\mathbf{r}) = \frac{\beta_a^2}{2} \frac{x^4 + y^4}{r^2} + \frac{\alpha_a^2}{2} \frac{z^4}{r^2} + \beta_a^2 \frac{x^2 y^2}{r^2} - \alpha_a \beta_a \frac{(x^2 + y^2) z^2}{r^2}. \tag{B5}$$

The angular integration of $f_a^{(1)}$ and $f_a^{(2)}$ can be performed analytically as

$$F_a^{(1)}(r) := \int f_a^{(1)}(\mathbf{r}) d\Omega = \frac{2\pi}{15} r (17\alpha_a^2 - 36\alpha_a \beta_a + 52\beta_a^2 - 10\alpha_a + 20\beta_a), \tag{B6}$$

$$F_a^{(2)}(r) := \int f_a^{(2)}(\mathbf{r}) d\Omega = \frac{2\pi}{15} r^2 (3\alpha_a^2 - 4\alpha_a \beta_a + 8\beta_a^2), \tag{B7}$$

respectively. Let us consider using this transformation how the energy of the system changes when an infinitesimal quadrupole deformation $|\alpha_a| \ll 1$ and $|\beta_a| \ll 1$ is induced to a spherically symmetric system $\rho_{\text{sph}}(\mathbf{r}) = \rho_{\text{sph}}(r)$.

Kinetic energy—The kinetic energy reads

$$\begin{aligned}
T_{\text{def}, a} &= \langle \Psi_{\text{def}, a} | \hat{T} | \Psi_{\text{def}, a} \rangle \\
&= \left(\frac{2}{3} e^{2\beta_a} + \frac{1}{3} e^{-2\alpha_a} \right) \langle \Psi_{\text{sph}, a} | \hat{T} | \Psi_{\text{sph}, a} \rangle \\
&= \left(\frac{2}{3} e^{2\beta_a} + \frac{1}{3} e^{-2\alpha_a} \right) T_{\text{sph}, a}. \tag{B8}
\end{aligned}$$

Central external potential energy—By using Eq. (B3) and the angular integral Eqs. (B6) and (B7), the central external potential changes as

$$\begin{aligned}
& \Delta E_{\text{ext},a} \\
& \simeq \left[(2\beta_a - \alpha_a) + \frac{1}{2} (2\beta_a - \alpha_a)^2 \right] \int \rho_{\text{sph},a}(r) V_{\text{ext}}(r) d\mathbf{r} \\
& \quad + \int f_a^{(1)}(\mathbf{r}) \frac{d\rho_{\text{sph},a}(r)}{dr} V_{\text{ext}}(r) d\mathbf{r} + \int f_a^{(2)}(\mathbf{r}) \frac{d^2\rho_{\text{sph},a}(r)}{dr^2} V_{\text{ext}}(r) d\mathbf{r} \\
& = 4\pi \left[(2\beta_a - \alpha_a) + \frac{1}{2} (2\beta_a - \alpha_a)^2 \right] \int_0^\infty \rho_{\text{sph},a}(r) V_{\text{ext}}(r) r^2 dr \\
& \quad + \int_0^\infty F_a^{(1)}(r) \frac{d\rho_{\text{sph},a}(r)}{dr} V_{\text{ext}}(r) r^2 dr + \int_0^\infty F_a^{(2)}(r) \frac{d^2\rho_{\text{sph},a}(r)}{dr^2} V_{\text{ext}}(r) r^2 dr \\
& = 4\pi \left[(2\beta_a - \alpha_a) + \frac{1}{2} (2\beta_a - \alpha_a)^2 \right] \int_0^\infty \rho_{\text{sph},a}(r) V_{\text{ext}}(r) r^2 dr \\
& \quad - \int_0^\infty \rho_{\text{sph},a}(r) \frac{d}{dr} \left[F_a^{(1)}(r) V_{\text{ext}}(r) r^2 \right] dr + \int_0^\infty \rho_{\text{sph},a}(r) \frac{d^2}{dr^2} \left[F_a^{(2)}(r) V_{\text{ext}}(r) r^2 \right] dr,
\end{aligned} \tag{B9}$$

where the external potential $V_{\text{ext}}(r) \sim r^d$ ($d > -3$) is assumed to behave as $r \rightarrow 0$. We assume the form of the external potential as $V_{\text{ext}}(r) = cr^d$ with given constants c and d . Substituting this form into Eq. (B9), we get

$$\begin{aligned}
\Delta E_{\text{ext},a} = & \left[- (2\beta_a - \alpha_a) + \frac{1}{2} (2\beta_a - \alpha_a)^2 \right. \\
& - \frac{1}{30} (d+3) (17\alpha_a^2 - 36\alpha_a\beta_a + 52\beta_a^2 - 10\alpha_a + 20\beta_a) \\
& \left. + \frac{1}{30} (d+4) (d+3) (3\alpha_a^2 - 4\alpha_a\beta_a + 8\beta_a^2) \right] E_{\text{ext},a}^{\text{sph}}.
\end{aligned} \tag{B10}$$

In the case of the Coulomb potential ($d = -1$), Eq. (B10) reads

$$\begin{aligned}
& \Delta E_{\text{ext},a} \\
& = \left[- (2\beta_a - \alpha_a) + \frac{1}{2} (2\beta_a - \alpha_a)^2 - \frac{1}{15} (8\alpha_a^2 - 24\alpha_a\beta_a + 28\beta_a^2 - 10\alpha_a + 20\beta_a) \right] E_{\text{ext},a}^{\text{sph}},
\end{aligned} \tag{B11}$$

while in the case of the harmonic oscillator potential ($d = 2$), Eq. (B10) reads

$$\begin{aligned}
& \Delta E_{\text{ext},a} \\
& = \left[- (2\beta_a - \alpha_a) + \frac{1}{2} (2\beta_a - \alpha_a)^2 + \frac{1}{6} (\alpha_a^2 + 12\alpha_a\beta_a - 4\beta_a^2 - 10\alpha_a + 20\beta_a) \right] E_{\text{ext},a}^{\text{sph}}.
\end{aligned} \tag{B12}$$

Interaction energy—Substituting Eqs. (B3) and (4.18) into Eq. (4.17), one obtains

$$\begin{aligned}
E_{\text{int}, ab}^{\text{def}} &\simeq c_a c_b E_{\text{int}, ab}^{\text{sph}} \\
&+ \frac{c_a}{2} \int_0^\infty \int_0^\infty F_b^{(1)}(r') \rho_{\text{sph}, a}(r) \frac{d\rho_{\text{sph}, b}(r')}{dr'} V_0^{ab}(r, r') r^2 r'^2 dr dr' \\
&+ \frac{c_b}{2} \int_0^\infty \int_0^\infty F_a^{(1)}(r) \frac{d\rho_{\text{sph}, a}(r)}{dr} \rho_{\text{sph}, b}(r') V_0^{ab}(r, r') r^2 r'^2 dr dr' \\
&+ \frac{c_a}{2} \int_0^\infty \int_0^\infty F_b^{(2)}(r') \rho_{\text{sph}, a}(r) \frac{d^2 \rho_{\text{sph}, b}(r')}{dr'^2} V_0^{ab}(r, r') r^2 r'^2 dr dr' \\
&+ \frac{c_b}{2} \int_0^\infty \int_0^\infty F_a^{(2)}(r) \frac{d^2 \rho_{\text{sph}, a}(r)}{dr^2} \rho_{\text{sph}, b}(r') V_0^{ab}(r, r') r^2 r'^2 dr dr' \\
&+ \frac{1}{8\pi} \int_0^\infty \int_0^\infty F_a^{(1)}(r) F_b^{(1)}(r') \frac{d\rho_{\text{sph}, a}(r)}{dr} \frac{d\rho_{\text{sph}, b}(r')}{dr'} V_0^{ab}(r, r') r^2 r'^2 dr dr' \\
&+ \frac{8\pi}{45} (\alpha_a + \beta_a) (\alpha_b + \beta_b) \int_0^\infty \int_0^\infty \frac{d\rho_{\text{sph}, a}(r)}{dr} \frac{d\rho_{\text{sph}, b}(r')}{dr'} V_2^{ab}(r, r') r^3 r'^3 dr dr', \tag{B13}
\end{aligned}$$

where $c_a = 1 + (2\beta_a - \alpha_a) + \frac{1}{2}(2\beta_a - \alpha_a)^2$.

In the case of atomic nuclei, substituting Eq. (4.23) into Eq. (B13), one obtains

$$\begin{aligned}
E_{\text{int}, ab}^{\text{def}} &\simeq c_a c_b E_{\text{int}, ab}^{\text{sph}} \\
&- \frac{\pi c_a g_{ab}}{15} (17\alpha_b^2 - 36\alpha_b \beta_b + 52\beta_b^2 - 10\alpha_b + 20\beta_b) \int_0^\infty \rho_{\text{sph}, a}(r) \frac{d\rho_{\text{sph}, b}(r)}{dr} r^3 dr \\
&- \frac{\pi c_b g_{ab}}{15} (17\alpha_a^2 - 36\alpha_a \beta_a + 52\beta_a^2 - 10\alpha_a + 20\beta_a) \int_0^\infty \rho_{\text{sph}, b}(r) \frac{d\rho_{\text{sph}, a}(r)}{dr} r^3 dr \\
&- \frac{\pi c_a g_{ab}}{15} (3\alpha_b^2 - 4\alpha_b \beta_b + 8\beta_b^2) \int_0^\infty \rho_{\text{sph}, a}(r) \frac{d^2 \rho_{\text{sph}, b}(r)}{dr^2} r^4 dr \\
&- \frac{\pi c_b g_{ab}}{15} (3\alpha_a^2 - 4\alpha_a \beta_a + 8\beta_a^2) \int_0^\infty \rho_{\text{sph}, b}(r) \frac{d^2 \rho_{\text{sph}, a}(r)}{dr^2} r^4 dr \\
&- \frac{\pi g_{ab}}{450} (17\alpha_a^2 - 36\alpha_a \beta_a + 52\beta_a^2 - 10\alpha_a + 20\beta_a) \\
&\quad \times (17\alpha_b^2 - 36\alpha_b \beta_b + 52\beta_b^2 - 10\alpha_b + 20\beta_b) \int_0^\infty \frac{d\rho_{\text{sph}, a}(r)}{dr} \frac{d\rho_{\text{sph}, b}(r)}{dr} r^4 dr \\
&- \frac{8\pi g_{ab}}{45} (\alpha_a + \beta_a) (\alpha_b + \beta_b) \int_0^\infty \frac{d\rho_{\text{sph}, a}(r)}{dr} \frac{d\rho_{\text{sph}, b}(r)}{dr} r^4 dr. \tag{B14}
\end{aligned}$$

In the case of atoms, substituting Eq. (4.25) into Eq. (B13), one obtains

$$\begin{aligned}
E_{\text{int},ab}^{\text{def}} &\simeq c_a c_b E_{\text{int},ab}^{\text{sph}} \\
&+ \frac{4\pi^2 c_a}{15} (17\alpha_b^2 - 36\alpha_b \beta_b + 52\beta_b^2 - 10\alpha_b + 20\beta_b) \\
&\quad \times \int_0^\infty \int_0^\infty \rho_{\text{sph},a}(r) \frac{d\rho_{\text{sph},b}(r')}{dr'} \frac{1}{r_>} r^2 r'^3 dr dr' \\
&+ \frac{4\pi^2 c_b}{15} (17\alpha_a^2 - 36\alpha_a \beta_a + 52\beta_a^2 - 10\alpha_a + 20\beta_a) \\
&\quad \times \int_0^\infty \int_0^\infty \frac{d\rho_{\text{sph},a}(r)}{dr} \rho_{\text{sph},b}(r') \frac{1}{r_>} r^3 r'^2 dr dr' \\
&+ \frac{4\pi^2 c_a}{15} (3\alpha_b^2 - 4\alpha_b \beta_b + 8\beta_b^2) \int_0^\infty \int_0^\infty \rho_{\text{sph},a}(r) \frac{d^2 \rho_{\text{sph},b}(r')}{dr'^2} \frac{1}{r_>} r^2 r'^4 dr dr' \\
&+ \frac{4\pi^2 c_b}{15} (3\alpha_a^2 - 4\alpha_a \beta_a + 8\beta_a^2) \int_0^\infty \int_0^\infty \frac{d^2 \rho_{\text{sph},a}(r)}{dr^2} \rho_{\text{sph},b}(r') \frac{1}{r_>} r^4 r'^2 dr dr' \\
&+ \frac{2\pi^2}{225} (17\alpha_a^2 - 36\alpha_a \beta_a + 52\beta_a^2 - 10\alpha_a + 20\beta_a) \\
&\quad \times (17\alpha_b^2 - 36\alpha_b \beta_b + 52\beta_b^2 - 10\alpha_b + 20\beta_b) \\
&\quad \times \int_0^\infty \int_0^\infty \frac{d\rho_{\text{sph},a}(r)}{dr} \frac{d\rho_{\text{sph},b}(r')}{dr'} \frac{1}{r_>} r^3 r'^3 dr dr' \\
&+ \frac{32\pi^2}{225} (\alpha_a + \beta_a) (\alpha_b + \beta_b) \int_0^\infty \int_0^\infty \frac{d\rho_{\text{sph},a}(r)}{dr} \frac{d\rho_{\text{sph},b}(r')}{dr'} \frac{r_{\leq}^2}{r_{>}^3} r^3 r'^3 dr dr'. \quad (\text{B15})
\end{aligned}$$

Substituting $\alpha_a = 2\beta_a$ into equations shown here, one can obtain equations shown in Sec. 4. As long as the small deformation is considered, the conclusion shown in Sec. 4 remains.

C. Numerical data

All the numerical data related to the main part of the paper are shown in Tables C1–C10.

Table C1 The root-mean radii, $Z \langle r^2 \rangle$, the quadrupole moments, Q , and the deformation parameters, β , calculated with the unrestricted Hartree-Fock method with the 6-31+G basis. Configurations of the valence electrons calculated by the natural orbital analysis are also shown.

Atom	Z	Mult.	Energy	$Z \langle r^2 \rangle$	Q_x	Q_y	Q_z	β_x	β_y	β_z	Config.
Li	3	2	-7.4315	18.2800	0.0000	0.0000	0.0000	0.0000	0.0000	0.0000	$2s^{1.00}$
Be	4	1	-14.5696	17.3430	0.0000	0.0000	0.0000	0.0000	0.0000	0.0000	$2s^{2.00}$
B	5	2	-24.5237	15.9020	-2.4718	-2.4718	+4.9435	-0.1232	-0.1232	+0.2464	$2s^{2.00} 2p^{1.00}$
C	6	3	-37.6809	13.8214	+1.4877	+1.4877	-2.9754	+0.0853	+0.0853	-0.1706	$2s^{2.00} 2p^{2.00}$
N	7	4	-54.3863	12.1756	0.0000	0.0000	0.0000	0.0000	0.0000	0.0000	$2s^{2.00} 2p^{3.00}$
O	8	3	-74.7835	11.3088	-0.9747	-0.9747	+1.9496	-0.0683	-0.0683	+0.1367	$2s^{2.00} 2p^{3.99} 3p^{0.01}$
F	9	2	-99.3675	10.3172	+0.6952	+0.6952	-1.3904	+0.0534	+0.0534	-0.1068	$2s^{2.00} 2p^{5.00}$
Ne	10	1	-128.4835	9.4321	0.0000	0.0000	0.0000	0.0000	0.0000	0.0000	$2s^{2.00} 2p^{6.00}$
Na	11	2	-161.8414	27.1816	0.0000	0.0000	0.0000	0.0000	0.0000	0.0000	$3s^{1.00}$
Mg	12	1	-199.5953	29.6206	0.0000	0.0000	0.0000	0.0000	0.0000	0.0000	$3s^{2.00}$
Al	13	2	-241.8545	33.4055	-5.5694	-5.5694	+11.1387	-0.1322	-0.1322	+0.2643	$3s^{2.00} 3p^{1.00}$
Si	14	3	-288.8288	32.2974	+3.5934	+3.5934	-7.1869	+0.0882	+0.0882	-0.1764	$3s^{2.00} 3p^{2.00}$
P	15	4	-340.6894	30.3267	0.0000	0.0000	0.0000	0.0000	0.0000	0.0000	$3s^{2.00} 3p^{3.00}$
S	16	3	-397.4722	29.2999	-2.3199	-2.3199	+4.6397	-0.0628	-0.0628	+0.1255	$3s^{2.00} 3p^{4.00}$
Cl	17	2	-459.4438	27.7141	+1.7509	+1.7509	-3.5020	+0.0501	+0.0501	-0.1002	$3s^{2.00} 3p^{5.00}$
Ar	18	1	-526.7731	26.0836	0.0000	0.0000	0.0000	0.0000	0.0000	0.0000	$3s^{2.00} 3p^{6.00}$
K	19	2	-599.1190	51.2038	0.0000	0.0000	0.0000	0.0000	0.0000	0.0000	$4s^{1.00}$
Ca	20	1	-676.7079	56.6004	0.0000	0.0000	0.0000	0.0000	0.0000	0.0000	$4s^{2.00}$
Sc	21	2	-759.6763	53.1310	+0.2094	+0.2094	-0.4189	+0.0031	+0.0031	-0.0062	$4s^{1.99} 3d^{1.00}$
Ti	22	3	-848.3215	50.2245	-0.1626	-0.1626	+0.3250	-0.0026	-0.0026	+0.0051	$4s^{1.99} 3d^{2.00}$
V	23	4	-942.7941	47.6799	0.0000	0.0000	0.0000	0.0000	0.0000	0.0000	$4s^{1.99} 3d^{3.00} 5s^{0.01}$
Cr	24	7	-1043.2424	37.9685	0.0000	0.0000	0.0000	0.0000	0.0000	0.0000	$4s^{1.00} 3d^{5.00}$
Mn	25	6	-1149.6148	37.0228	+0.7490	+0.7490	-1.4982	+0.0160	+0.0160	-0.0321	$4s^{1.00} 3d^{5.98} 4d^{0.02}$
Fe	26	5	-1262.2043	35.7532	-0.5400	-0.5400	+1.0797	-0.0120	-0.0120	+0.0239	$4s^{1.00} 3d^{6.99} 4d^{0.01}$
Co	27	4	-1381.1643	34.5419	0.0000	0.0000	0.0000	0.0000	0.0000	0.0000	$4s^{1.00} 3d^{8.00}$
Ni	28	3	-1506.5944	33.4315	-0.4075	-0.4075	+0.8148	-0.0097	-0.0097	+0.0193	$4s^{1.00} 3d^{9.00}$
Cu	29	2	-1638.6938	32.2616	0.0000	0.0000	0.0000	0.0000	0.0000	0.0000	$4s^{1.00} 3d^{10.00}$
Zn	30	1	-1777.5332	35.0221	0.0000	0.0000	0.0000	0.0000	0.0000	0.0000	$4s^{2.00} 3d^{10.00}$
Ga	31	2	-1921.1399	41.4244	-5.5787	-5.5787	+11.1575	-0.1068	-0.1068	+0.2135	$4s^{2.00} 4p^{1.00}$
Ge	32	3	-2073.0829	42.1351	+3.9175	+3.9175	-7.8353	+0.0737	+0.0737	-0.1474	$4s^{2.00} 4p^{2.00}$
As	33	4	-2231.8086	41.4771	0.0000	0.0000	0.0000	0.0000	0.0000	0.0000	$4s^{2.00} 4p^{3.00}$
Se	34	3	-2397.3677	41.6200	-2.8141	-2.8141	+5.6285	-0.0536	-0.0536	+0.1072	$4s^{2.00} 4p^{4.00}$
Br	35	2	-2569.7593	40.7722	+2.2376	+2.2376	-4.4751	+0.0435	+0.0435	-0.0870	$4s^{2.00} 4p^{5.00}$
Kr	36	1	-2749.2009	39.7020	0.0000	0.0000	0.0000	0.0000	0.0000	0.0000	$4s^{2.00} 4p^{6.00}$

Table C2 Same as Table C1, but with the dAug-CC-pV5Z basis.

Atom	Z	Mult.	Energy	$Z \langle r^2 \rangle$	Q_x	Q_y	Q_z	β_x	β_y	β_z	Config.
Li	3	2	-7.4327	18.6252	0.0000	0.0000	0.0000	0.0000	0.0000	0.0000	$2s^{1.00}$
Be	4	1	-14.5730	17.3210	0.0000	0.0000	0.0000	0.0000	0.0000	0.0000	$2s^{2.00}$
B	5	2	-24.5331	15.7731	-2.4912	-2.4912	+4.9823	-0.1252	-0.1252	+0.2504	$2s^{1.99} 2p^{1.00} 3d^{0.01}$
C	6	3	-37.6937	13.7574	+1.4846	+1.4846	-2.9689	+0.0855	+0.0855	-0.1711	$2s^{1.99} 2p^{2.00}$
N	7	4	-54.4045	12.0782	0.0000	0.0000	0.0000	0.0000	0.0000	0.0000	$2s^{2.00} 2p^{3.00}$
O	8	3	-74.8188	11.2130	-0.9517	-0.9517	+1.9037	-0.0673	-0.0673	+0.1346	$2s^{2.00} 2p^{3.99} 3p^{0.01}$
F	9	2	-99.4161	10.2470	+0.6738	+0.6738	-1.3476	+0.0521	+0.0521	-0.1042	$2s^{2.00} 2p^{5.00}$
Ne	10	1	-128.5468	9.3741	0.0000	0.0000	0.0000	0.0000	0.0000	0.0000	$2s^{2.00} 2p^{6.00}$
Na	11	2	-161.8587	27.1413	0.0000	0.0000	0.0000	0.0000	0.0000	0.0000	$3s^{1.00}$
Al	13	2	-241.8807	33.1885	-5.7634	-5.7634	+11.5268	-0.1377	-0.1377	+0.2753	$3s^{1.99} 3p^{1.00} 3d^{0.01}$
Si	14	3	-288.8588	32.1436	+3.6302	+3.6302	-7.2605	+0.0895	+0.0895	-0.1790	$3s^{1.99} 3p^{2.00} 3d^{0.01}$
P	15	4	-340.7192	30.2655	0.0000	0.0000	0.0000	0.0000	0.0000	0.0000	$3s^{2.00} 3p^{3.00}$
S	16	3	-397.5132	29.1710	-2.1695	-2.1695	+4.3391	-0.0590	-0.0590	+0.1179	$3s^{1.99} 3p^{4.00} 3d^{0.01}$
Cl	17	2	-459.4897	27.6256	+1.6258	+1.6258	-3.2517	+0.0466	+0.0466	-0.0933	$3s^{2.00} 3p^{5.00}$
Ar	18	1	-526.8173	26.0376	0.0000	0.0000	0.0000	0.0000	0.0000	0.0000	$3s^{2.00} 3p^{6.00}$
Sc	21	2	-759.7408	53.1077	+0.1976	+0.1976	-0.3955	+0.0029	+0.0029	-0.0059	$4s^{1.99} 3d^{1.00}$
Ti	22	3	-848.4026	50.2023	-0.1508	-0.1508	+0.3016	-0.0024	-0.0024	+0.0048	$4s^{2.00} 3d^{2.00}$
V	23	4	-942.8935	47.6556	0.0000	0.0000	0.0000	0.0000	0.0000	0.0000	$4s^{1.99} 3d^{3.00} 5s^{0.01}$
Cr	24	7	-1043.3567	37.6585	0.0000	0.0000	0.0000	0.0000	0.0000	0.0000	$4s^{1.00} 3d^{5.00}$
Mn	25	6	-1149.7533	36.7555	+0.6276	+0.6276	-1.2551	+0.0135	+0.0135	-0.0271	$4s^{1.00} 3d^{5.99} 4d^{0.01}$
Fe	26	5	-1262.3743	35.4942	-0.4318	-0.4318	+0.8636	-0.0096	-0.0096	+0.0193	$4s^{1.00} 3d^{6.99} 4d^{0.01}$
Co	27	4	-1381.3674	34.2853	0.0000	0.0000	0.0000	0.0000	0.0000	0.0000	$4s^{1.00} 3d^{8.00}$
Ni	28	3	-1506.8305	33.1827	+0.2806	+0.3348	-0.6154	+0.0067	+0.0080	-0.0147	$4s^{1.00} 3d^{9.00}$
Cu	29	2	-1638.9574	36.3225	-0.0156	-0.2304	+0.2462	0.0003	-0.0050	+0.0054	$4s^{2.00} 3d^{9.00}$
Zn	30	1	-1777.8480	34.9792	0.0000	0.0000	0.0000	0.0000	0.0000	0.0000	$4s^{2.00} 3d^{10.00}$
Ga	31	2	-1923.2644	40.7328	-5.6952	-5.6952	+11.3903	-0.1108	-0.1108	+0.2217	$4s^{1.99} 4p^{1.00} 4d^{0.01}$
Ge	32	3	-2075.3638	41.5004	+3.9233	+3.9233	-7.8466	+0.0749	+0.0749	-0.1499	$4s^{1.99} 4p^{2.00} 4d^{0.01}$
As	33	4	-2234.2398	41.0402	0.0000	0.0000	0.0000	0.0000	0.0000	0.0000	$4s^{2.00} 4p^{3.00}$
Se	34	3	-2399.8753	41.1769	-2.5759	-2.5759	+5.1518	-0.0496	-0.0496	+0.0992	$4s^{2.00} 4p^{4.00}$
Br	35	2	-2572.4483	40.5058	+2.0362	+2.0362	-4.0723	+0.0398	+0.0398	-0.0797	$4s^{2.00} 4p^{5.00}$
Kr	36	1	-2752.0549	39.5314	0.0000	0.0000	0.0000	0.0000	0.0000	0.0000	$4s^{2.00} 4p^{6.00}$

Table C3 Same as Table C1, but with the STO-3G basis.

Atom	Z	Mult.	Energy	$Z \langle r^{-2} \rangle$	Q_x	Q_y	Q_z	β_x	β_y	β_z	Config.
Li	3	2	-7.3155	13.0955	0.0000	0.0000	0.0000	0.0000	0.0000	0.0000	2s ^{1.00}
Be	4	1	-14.3519	12.3657	0.0000	0.0000	0.0000	0.0000	0.0000	0.0000	2s ^{2.00}
B	5	2	-24.1490	10.6497	-1.3369	-1.3369	+2.6738	-0.0995	-0.0995	+0.1990	2s ^{2.00} 2p ^{1.00}
C	6	3	-37.1984	10.5788	+1.0169	+1.0169	-2.0335	+0.0762	+0.0762	-0.1524	2s ^{2.00} 2p ^{2.00}
N	7	4	-53.7190	10.1785	0.0000	0.0000	0.0000	0.0000	0.0000	0.0000	2s ^{2.00} 2p ^{3.00}
O	8	3	-73.8042	9.1334	-0.5942	-0.5942	+1.1884	-0.0516	-0.0516	+0.1031	2s ^{2.00} 2p ^{4.00}
F	9	2	-97.9865	8.2689	+0.4626	+0.4626	-0.9252	+0.0443	+0.0443	-0.0887	2s ^{2.00} 2p ^{5.00}
Ne	10	1	-126.6045	7.3940	0.0000	0.0000	0.0000	0.0000	0.0000	0.0000	2s ^{2.00} 2p ^{6.00}
Na	11	2	-159.6684	12.1291	0.0000	0.0000	0.0000	0.0000	0.0000	0.0000	3s ^{1.00}
Mg	12	1	-197.0074	15.6258	0.0000	0.0000	0.0000	0.0000	0.0000	0.0000	3s ^{2.00}
Al	13	2	-238.8584	19.1823	-2.0286	-2.0286	+4.0571	-0.0838	-0.0838	+0.1677	3s ^{2.00} 3p ^{1.00}
Si	14	3	-285.4662	22.0780	+1.9050	+1.9050	-3.8102	+0.0684	+0.0684	-0.1368	3s ^{2.00} 3p ^{2.00}
P	15	4	-336.8688	22.6495	0.0000	0.0000	0.0000	0.0000	0.0000	0.0000	3s ^{2.00} 3p ^{3.00}
S	16	3	-393.1302	22.8523	-1.3907	-1.3907	+2.7811	-0.0482	-0.0482	+0.0965	3s ^{2.00} 3p ^{4.00}
Cl	17	2	-454.5422	24.7260	+1.3180	+1.3180	-2.6361	+0.0423	+0.0423	-0.0845	3s ^{2.00} 3p ^{5.00}
Ar	18	1	-521.2229	22.9344	0.0000	0.0000	0.0000	0.0000	0.0000	0.0000	3s ^{2.00} 3p ^{6.00}
K	19	2	-593.0778	33.1098	0.0000	0.0000	0.0000	0.0000	0.0000	0.0000	4s ^{1.00}
Ca	20	1	-669.9889	42.2174	0.0000	0.0000	0.0000	0.0000	0.0000	0.0000	4s ^{2.00}
Sc	21	2	-751.9936	44.3275	+2.4323	+2.4323	-4.8643	+0.0435	+0.0435	-0.0870	4s ^{1.98} 3d ^{1.02}
Ti	22	3	-839.5552	36.4583	-0.8418	-0.8418	+1.6833	-0.0183	-0.0183	+0.0366	4s ^{1.99} 3d ^{2.01}
V	23	4	-932.3822	51.8131	0.0000	0.0000	0.0000	0.0000	0.0000	0.0000	4s ^{2.00} 4p ^{3.00}
Cr	24	7	-1031.9037	43.3117	-0.4164	-0.4164	+0.8326	-0.0076	-0.0076	+0.0152	4s ^{1.00} 3d ^{2.00} 4p ^{3.00}
Mn	25	6	-1137.6484	31.6207	0.0000	0.0000	0.0000	0.0000	0.0000	0.0000	4s ^{2.00} 3d ^{5.00}
Fe	26	5	-1249.0414	41.1316	-3.8513	-3.8513	+7.7028	-0.0742	-0.0742	+0.1484	4s ^{2.00} 3d ^{5.00} 4p ^{1.00}
Co	27	4	-1366.3895	48.9607	+3.8432	+3.8432	-7.6865	+0.0622	+0.0622	-0.1244	4s ^{2.00} 3d ^{5.00} 4p ^{2.00}
Ni	28	3	-1490.1299	46.3092	+3.8145	+3.8145	-7.6292	+0.0653	+0.0653	-0.1306	4s ^{2.00} 3d ^{6.00} 4p ^{2.00}
Cu	29	2	-1620.3878	37.6504	-3.5702	-3.5702	+7.1405	-0.0752	-0.0752	+0.1503	4s ^{2.00} 3d ^{8.00} 4p ^{1.00}
Zn	30	1	-1757.1763	35.4563	-4.8110	-4.8110	+9.6221	-0.1076	-0.1076	+0.2151	4s ^{2.00} 3d ^{8.00} 4p ^{2.00}
Ga	31	2	-1900.7285	31.3321	-2.8420	-2.8420	+5.6842	-0.0719	-0.0719	+0.1438	4s ^{2.00} 4p ^{1.00}
Ge	32	3	-2051.6363	32.0788	+2.3143	+2.3143	-4.6288	+0.0572	+0.0572	-0.1144	4s ^{2.00} 4p ^{2.00}
As	33	4	-2209.2637	33.7744	0.0000	0.0000	0.0000	0.0000	0.0000	0.0000	4s ^{2.00} 4p ^{3.00}
Se	34	3	-2373.5273	35.4117	-1.8814	-1.8814	+3.7627	-0.0421	-0.0421	+0.0842	4s ^{2.00} 4p ^{4.00}
Br	35	2	-2544.6368	35.2509	+1.6414	+1.6414	-3.2825	+0.0369	+0.0369	-0.0738	4s ^{2.00} 4p ^{5.00}
Kr	36	1	-2722.7060	34.8481	0.0000	0.0000	0.0000	0.0000	0.0000	0.0000	4s ^{2.00} 4p ^{6.00}
Rb	37	2	-2907.6043	44.3734	0.0000	0.0000	0.0000	0.0000	0.0000	0.0000	5s ^{1.00}
Sr	38	1	-3099.1167	51.3762	0.0000	0.0000	0.0000	0.0000	0.0000	0.0000	5s ^{2.00}
Y	39	2	-3297.3418	58.4961	+0.9769	+0.9769	-1.9539	+0.0132	+0.0132	-0.0265	5s ^{1.72} 4d ^{1.28}
Zr	40	3	-3503.0360	53.2014	-1.2644	-1.2644	+2.5289	-0.0188	-0.0188	+0.0377	5s ^{1.81} 4d ^{2.19}
Nb	41	6	-3715.8900	45.9028	+1.1380	+1.1380	-2.2759	+0.0197	+0.0197	-0.0393	5s ^{1.00} 4d ^{4.00}
Mo	42	7	-3935.8966	43.4772	0.0000	0.0000	0.0000	0.0000	0.0000	0.0000	5s ^{1.00} 4d ^{5.00}
Tc	43	6	-4163.2052	49.5440	0.0000	0.0000	0.0000	0.0000	0.0000	0.0000	5s ^{2.00} 4d ^{5.00}
Ru	44	5	-4397.7215	50.7468	+0.6444	+0.6444	-1.2887	+0.0101	+0.0101	-0.0201	5s ^{2.00} 4d ^{6.00}
Rh	45	4	-4639.7207	49.6014	-0.5554	-0.5554	+1.1108	-0.0089	-0.0089	+0.0178	5s ^{2.00} 4d ^{7.00}
Pd	46	1	-4889.1921	48.0030	+0.9705	+0.9705	-1.9409	+0.0160	+0.0160	-0.0321	5s ^{2.00} 4d ^{8.00}
Ag	47	2	-5146.5464	47.5080	-0.6013	-0.6013	+0.9283	-0.0100	-0.0100	+0.0155	5s ^{2.00} 4d ^{9.00}
Cd	48	1	-5411.5327	41.7214	0.0000	0.0000	0.0000	0.0000	0.0000	0.0000	5s ^{2.00} 4d ^{10.00}
In	49	2	-5682.7774	47.0137	-3.2899	-3.2899	+6.5798	-0.0555	-0.0555	+0.1109	5s ^{2.00} 5p ^{1.00}
Sn	50	3	-5963.2061	50.2820	+2.9919	+2.9919	-5.9838	+0.0472	+0.0472	-0.0943	5s ^{2.00} 5p ^{2.00}
Sb	51	4	-6251.3625	54.2873	0.0000	0.0000	0.0000	0.0000	0.0000	0.0000	5s ^{2.00} 5p ^{3.00}
Te	52	3	-6547.1224	56.9144	-2.6502	-2.6502	+5.3004	-0.0369	-0.0369	+0.0738	5s ^{2.00} 5p ^{4.00}
I	53	2	-6850.6762	57.2039	+2.3607	+2.3607	-4.7214	+0.0327	+0.0327	-0.0654	5s ^{2.00} 5p ^{5.00}
Xe	54	1	-7162.1042	56.8048	0.0000	0.0000	0.0000	0.0000	0.0000	0.0000	5s ^{2.00} 5p ^{6.00}

Table C4 The root-mean radii, $Z\langle r^2 \rangle$, the quadrupole moments, Q , and the deformation parameters, β , for Al, Cu, and Ga calculated with the several many-body calculation methods with the 6-31+G basis. Configurations of the valence electrons calculated by the natural orbital analysis are also shown.

Atom	Method	Energy	$Z\langle r^2 \rangle$	Q_x	Q_y	Q_z	β_x	β_y	β_z	Config.
Al	UHF	-241.8545	33.4055	-5.5694	-5.5694	+11.1387	-0.1322	-0.1322	+0.2643	$3s^{2.00} 3p^{1.00} 4s^{0.00} 4p^{0.00}$
Al	CCD	-241.8839	33.8409	-5.7148	-5.7148	+11.4296	-0.1339	-0.1339	+0.2677	$3s^{1.91} 3p^{1.07} 4s^{0.01} 4p^{0.02}$
Al	CCSD	-241.8841	33.8935	-5.7422	-5.7422	+11.4842	-0.1343	-0.1343	+0.2686	$3s^{1.91} 3p^{1.07} 4s^{0.01} 4p^{0.02}$
Al	CID	-241.8839	33.8409	-5.7148	-5.7148	+11.4296	-0.1339	-0.1339	+0.2677	$3s^{1.91} 3p^{1.07} 4s^{0.01} 4p^{0.02}$
Al	CISD	-241.8840	33.8814	-5.7367	-5.7367	+11.4733	-0.1342	-0.1342	+0.2684	$3s^{1.91} 3p^{1.07} 4s^{0.01} 4p^{0.02}$
Al	MP2	-241.8717	33.7371	-5.7126	-5.7126	+11.4254	-0.1342	-0.1342	+0.2684	$3s^{1.97} 3p^{1.02} 4s^{0.00} 4p^{0.01}$
Al	MP3	-241.8791	33.8428	-5.7476	-5.7476	+11.4952	-0.1346	-0.1346	+0.2692	$3s^{1.94} 3p^{1.04} 4s^{0.00} 4p^{0.01}$
Al	MP4	-241.8822	33.8727	-5.7491	-5.7491	+11.4983	-0.1345	-0.1345	+0.2691	$3s^{1.92} 3p^{1.06} 4s^{0.01} 4p^{0.01}$
Al	LDA	-241.2799	32.8660	-5.5932	-5.5932	+11.1867	-0.1349	-0.1349	+0.2698	$3s^{2.00} 3p^{1.00} 4s^{0.00} 4p^{0.00}$
Cu	UHF	-1638.6938	32.2616	0.0000	0.0000	0.0000	0.0000	0.0000	0.0000	$3d^{10.00} 4s^{1.00} 4p^{0.00} 4d^{0.00}$
Cu	CCD	-1638.9170	32.2339	0.0000	0.0000	0.0000	0.0000	0.0000	0.0000	$3d^{9.91} 4s^{0.99} 4p^{0.02} 4d^{0.07}$
Cu	CCSD	-1638.9226	32.3642	0.0000	0.0000	0.0000	0.0000	0.0000	0.0000	$3d^{9.90} 4s^{0.99} 4p^{0.02} 4d^{0.08}$
Cu	CID	-1638.9035	32.2233	0.0000	0.0000	0.0000	0.0000	0.0000	0.0000	$3d^{9.93} 4s^{0.99} 4p^{0.01} 4d^{0.06}$
Cu	CISD	-1638.9101	32.2921	0.0000	0.0000	0.0000	0.0000	0.0000	0.0000	$3d^{9.91} 4s^{0.99} 4p^{0.02} 4d^{0.07}$
Cu	MP2	-1638.9657	32.4330	0.0000	0.0000	0.0000	0.0000	0.0000	0.0000	$3d^{9.88} 4s^{1.00} 4p^{0.01} 4d^{0.12}$
Cu	MP3	-1638.8891	32.1425	0.0000	0.0000	0.0000	0.0000	0.0000	0.0000	$3d^{9.95} 4s^{0.99} 4p^{0.01} 4d^{0.04}$
Cu	MP4	-1638.9490	32.5433	0.0000	0.0000	0.0000	0.0000	0.0000	0.0000	$3d^{9.84} 4s^{1.00} 4p^{0.02} 4d^{0.14}$
Cu	LDA	-1637.4831	31.5039	0.0000	0.0000	0.0000	0.0000	0.0000	0.0000	$3d^{10.00} 4s^{1.00} 4p^{0.00} 4d^{0.00}$
Ga	UHF	-1921.1399	41.4244	-5.5787	-5.5787	+11.1575	-0.1068	-0.1068	+0.2135	$4s^{2.00} 4p^{1.00} 5s^{0.00} 5p^{0.00}$
Ga	CCD	-1921.1686	41.7576	-5.6909	-5.6909	+11.3819	-0.1080	-0.1080	+0.2161	$4s^{1.92} 4p^{1.06} 5s^{0.01} 5p^{0.01}$
Ga	CCSD	-1921.1688	41.8071	-5.7146	-5.7146	+11.4292	-0.1083	-0.1083	+0.2167	$4s^{1.92} 4p^{1.06} 5s^{0.01} 5p^{0.02}$
Ga	CID	-1921.1686	41.7576	-5.6909	-5.6909	+11.3819	-0.1080	-0.1080	+0.2161	$4s^{1.92} 4p^{1.06} 5s^{0.01} 5p^{0.01}$
Ga	CISD	-1921.1688	41.7947	-5.7092	-5.7092	+11.4187	-0.1083	-0.1083	+0.2166	$4s^{1.92} 4p^{1.06} 5s^{0.01} 5p^{0.02}$
Ga	MP2	-1921.1576	41.6788	-5.6963	-5.6963	+11.3923	-0.1083	-0.1083	+0.2167	$4s^{1.97} 4p^{1.02} 5s^{0.00} 5p^{0.01}$
Ga	MP3	-1921.1646	41.7557	-5.7190	-5.7190	+11.4381	-0.1086	-0.1086	+0.2171	$4s^{1.95} 4p^{1.04} 5s^{0.00} 5p^{0.01}$
Ga	MP4	-1921.1673	41.7795	-5.7177	-5.7177	+11.4356	-0.1085	-0.1085	+0.2170	$4s^{1.93} 4p^{1.05} 5s^{0.01} 5p^{0.01}$
Ga	LDA	-1919.7297	40.5292	-5.6550	-5.6550	+11.3100	-0.1106	-0.1106	+0.2212	$4s^{2.00} 4p^{1.00} 5s^{0.00} 5p^{0.00}$

Table C5 Same as Table C4, but with the dAug-CC-pV5Z basis.

Atom	Method	Energy	$Z \langle r^{-2} \rangle$	Q_x	Q_y	Q_z	β_x	β_y	β_z	Config.
Al	UHF	-241.8807	33.1885	-5.7634	-5.7634	+11.5268	-0.1377	-0.1377	+0.2753	3s ^{1.99} 3p ^{1.00} 3d ^{0.01} 4p ^{0.00}
Al	CCD	-241.9324	32.5801	-5.2419	-5.2419	+10.4841	-0.1275	-0.1275	+0.2551	3s ^{1.90} 3p ^{1.05} 3d ^{0.03} 4p ^{0.01}
Al	CCSD	-241.9332	32.5620	-5.2529	-5.2529	+10.5055	-0.1279	-0.1279	+0.2557	3s ^{1.89} 3p ^{1.05} 3d ^{0.04} 4p ^{0.01}
Al	CID	-241.9324	32.5801	-5.2419	-5.2419	+10.4841	-0.1275	-0.1275	+0.2551	3s ^{1.90} 3p ^{1.05} 3d ^{0.03} 4p ^{0.01}
Al	CISD	-241.9333	32.5568	-5.2513	-5.2513	+10.5029	-0.1279	-0.1279	+0.2557	3s ^{1.89} 3p ^{1.06} 3d ^{0.04} 4p ^{0.01}
Al	MP2	-241.9199	32.8683	-5.4066	-5.4066	+10.8129	-0.1304	-0.1304	+0.2608	3s ^{1.95} 3p ^{1.02} 3d ^{0.02} 4p ^{0.01}
Al	MP3	-241.9283	32.7040	-5.2941	-5.2941	+10.5885	-0.1283	-0.1283	+0.2566	3s ^{1.92} 3p ^{1.03} 3d ^{0.03} 4p ^{0.01}
Al	MP4	-241.9314	32.6312	-5.2596	-5.2596	+10.5194	-0.1278	-0.1278	+0.2555	3s ^{1.91} 3p ^{1.04} 3d ^{0.03} 4p ^{0.01}
Al	LDA	-241.3109	32.9046	-5.4817	-5.4817	+10.9637	-0.1321	-0.1321	+0.2641	3s ^{2.00} 3p ^{1.00} 3d ^{0.00} 4p ^{0.00}
Cu	UHF	-1638.9574	36.3225	-0.0156	-0.2304	+0.2462	-0.0003	-0.0050	+0.0054	3d ^{9.00} 4s ^{2.00} 4p ^{0.00} 4d ^{0.00} 4f ^{0.00} 5s ^{0.00} 5p ^{0.00}
Cu	CCD	-1639.3940	34.4852	+0.1256	-0.2824	+0.1568	+0.0029	-0.0065	+0.0036	3d ^{8.91} 4s ^{1.91} 4p ^{0.09} 4d ^{0.05} 4f ^{0.02} 5s ^{0.00} 5p ^{0.01}
Cu	CCSD	-1639.3988	34.7050	+0.0187	-0.3167	+0.2980	+0.0004	-0.0072	+0.0068	3d ^{8.91} 4s ^{1.90} 4p ^{0.09} 4d ^{0.05} 4f ^{0.02} 5s ^{0.01} 5p ^{0.01}
Cu	CID	-1639.3686	34.6404	+0.0560	-0.2844	+0.2284	+0.0013	-0.0065	+0.0052	3d ^{8.93} 4s ^{1.96} 4p ^{0.04} 4d ^{0.04} 4f ^{0.02} 5s ^{0.00} 5p ^{0.00}
Cu	CISD	-1639.3717	34.6775	+0.0999	-0.2904	+0.1905	+0.0023	-0.0066	+0.0044	3d ^{8.92} 4s ^{1.96} 4p ^{0.04} 4d ^{0.04} 4f ^{0.02} 5s ^{0.00} 5p ^{0.00}
Cu	MP2	-1639.4302	34.3392	-0.1485	-0.2480	+0.3968	-0.0034	-0.0057	+0.0092	3d ^{8.89} 4s ^{1.95} 4p ^{0.05} 4d ^{0.07} 4f ^{0.02} 5s ^{0.00} 5p ^{0.00}
Cu	MP3	-1639.3866	34.4844	-0.0161	-0.2404	+0.2565	-0.0004	-0.0055	+0.0059	3d ^{8.92} 4s ^{1.92} 4p ^{0.08} 4d ^{0.04} 4f ^{0.02} 5s ^{0.00} 5p ^{0.01}
Cu	MP4	-1639.4025	34.5798	+0.0410	-0.2632	+0.2224	+0.0009	-0.0060	+0.0051	3d ^{8.90} 4s ^{1.91} 4p ^{0.09} 4d ^{0.06} 4f ^{0.02} 5s ^{0.00} 5p ^{0.01}
Cu	LDA	-1637.7692	31.2608	0.0000	0.0000	0.0000	0.0000	0.0000	0.0000	3d ^{10.00} 4s ^{1.00} 4p ^{0.00} 4d ^{0.00} 4f ^{0.00} 5s ^{0.00} 5p ^{0.00}
Ga	UHF	-1923.2644	40.7328	-5.6952	-5.6952	+11.3903	-0.1108	-0.1108	+0.2217	4s ^{1.99} 4p ^{1.00} 4d ^{0.01} 4f ^{0.00} 5s ^{0.00} 5p ^{0.00} 5d ^{0.00}
Ga	CCD	-1923.5235	39.7317	-5.1260	-5.1260	+10.2519	-0.1023	-0.1023	+0.2045	4s ^{1.92} 4p ^{1.04} 4d ^{0.04} 4f ^{0.01} 5s ^{0.00} 5p ^{0.01} 5d ^{0.01}
Ga	CCSD	-1923.5288	39.7447	-5.1447	-5.1447	+10.2892	-0.1026	-0.1026	+0.2052	4s ^{1.92} 4p ^{1.04} 4d ^{0.05} 4f ^{0.01} 5s ^{0.01} 5p ^{0.02} 5d ^{0.01}
Ga	CID	-1923.5088	39.7560	-5.2203	-5.2203	+10.4408	-0.1041	-0.1041	+0.2082	4s ^{1.95} 4p ^{1.03} 4d ^{0.04} 4f ^{0.01} 5s ^{0.00} 5p ^{0.01} 5d ^{0.01}
Ga	CISD	-1923.5141	39.7442	-5.2196	-5.2196	+10.4391	-0.1041	-0.1041	+0.2082	4s ^{1.94} 4p ^{1.03} 4d ^{0.04} 4f ^{0.01} 5s ^{0.00} 5p ^{0.01} 5d ^{0.01}
Ga	MP2	-1923.5387	39.7807	-5.1518	-5.1518	+10.3039	-0.1027	-0.1027	+0.2053	4s ^{1.95} 4p ^{1.02} 4d ^{0.05} 4f ^{0.01} 5s ^{0.00} 5p ^{0.01} 5d ^{0.01}
Ga	MP3	-1923.5151	39.8152	-5.1556	-5.1556	+10.3115	-0.1026	-0.1026	+0.2053	4s ^{1.93} 4p ^{1.03} 4d ^{0.04} 4f ^{0.01} 5s ^{0.00} 5p ^{0.01} 5d ^{0.01}
Ga	MP4	-1923.5338	39.7092	-5.1079	-5.1079	+10.2156	-0.1020	-0.1020	+0.2039	4s ^{1.92} 4p ^{1.04} 4d ^{0.06} 4f ^{0.01} 5s ^{0.00} 5p ^{0.02} 5d ^{0.01}
Ga	LDA	-1921.8127	39.9893	-5.4132	-5.4132	+10.8265	-0.1073	-0.1073	+0.2146	4s ^{2.00} 4p ^{1.00} 4d ^{0.00} 4f ^{0.00} 5s ^{0.00} 5p ^{0.00} 5d ^{0.00}

Table C6 The single-particle quadrupole moments $q_i^{(\text{sp})}$ and the single-particle root-mean-square radii $\langle r^2 \rangle_{nl}$ for the occupied orbitals in the Al atom calculated by the unrestricted Hartree-Fock method with the 6-31+G basis. The single-particle energy of each orbital, ε_j , and the corresponding orbital are also shown.

Spin	Orbital	ε_j	$\langle r^2 \rangle_{nl}$	$q_x^{(\text{sp})}$	$q_y^{(\text{sp})}$	$q_z^{(\text{sp})}$
α	1s	-58.4930	0.0195	0.0000	0.0000	0.0000
α	2s	-4.9115	0.4591	0.0000	0.0000	0.0000
α	2p _z	-3.2244	0.4535	-0.1814	-0.1814	+0.3628
α	2p _x	-3.2186	0.4561	+0.3648	-0.1824	-0.1824
α	2p _y	-3.2186	0.4561	-0.1824	+0.3648	-0.1824
α	3s	-0.4238	7.9466	0.0000	0.0000	0.0000
α	3p _z	-0.2099	13.9269	-5.5708	-5.5708	+11.1416
β	1s	-58.4903	0.0195	0.0000	0.0000	0.0000
β	2s	-4.9081	0.4588	0.0000	0.0000	0.0000
β	2p _x	-3.2173	0.4557	+0.3646	-0.1823	-0.1823
β	2p _y	-3.2173	0.4557	-0.1823	+0.3646	-0.1823
β	2p _z	-3.2080	0.4547	-0.1819	-0.1819	+0.3637
β	3s	-0.3628	7.8434	0.0000	0.0000	0.0000
Total			33.4055	-5.5693	-5.5693	+11.1387

Table C7 Same as Table C6, but for the Sc atom.

Spin	Orbital	ε_j	$\langle r^2 \rangle_{nl}$	$q_x^{(\text{sp})}$	$q_y^{(\text{sp})}$	$q_z^{(\text{sp})}$
α	1s	-165.8952	0.0073	0.0000	0.0000	0.0000
α	2s	-19.0956	0.1393	0.0000	0.0000	0.0000
α	2p _z	-15.6861	0.1162	-0.0465	-0.0465	+0.0930
α	2p _x	-15.6830	0.1164	+0.0931	-0.0466	-0.0466
α	2p _y	-15.6830	0.1164	-0.0466	+0.0931	-0.0466
α	3s	-2.5988	1.3396	+0.0016	+0.0016	-0.0031
α	3p _x	-1.6232	1.6265	+1.3012	-0.6506	-0.6506
α	3p _y	-1.6232	1.6265	-0.6506	+1.3012	-0.6506
α	3p _z	-1.5893	1.6107	-0.6443	-0.6443	+1.2886
α	3d _{xy}	-0.3375	3.7873	+1.0821	+1.0821	-2.1642
α	4s	-0.2171	17.4198	+0.1076	+0.1076	-0.2152
β	1s	-165.8951	0.0073	0.0000	0.0000	0.0000
β	2s	-19.0832	0.1391	-0.0001	-0.0001	+0.0001
β	2p _z	-15.6837	0.1162	-0.0465	-0.0465	+0.0929
β	2p _x	-15.6657	0.1161	+0.0929	-0.0464	-0.0464
β	2p _y	-15.6657	0.1161	-0.0464	+0.0929	-0.0464
β	3s	-2.5451	1.3370	-0.0194	-0.0194	+0.0387
β	3p _z	-1.5798	1.6156	-0.6462	-0.6462	+1.2925
β	3p _x	-1.5273	1.6196	+1.2957	-0.6478	-0.6478
β	3p _y	-1.5273	1.6196	-0.6478	+1.2957	-0.6478
β	4s	-0.2051	18.5388	-0.9703	-0.9703	+1.9406
Total			53.1312	+0.2095	+0.2095	-0.4189

Table C8 Same as Table C6, but for the Ti atom.

Spin	Orbital	ε_j	$\langle r^2 \rangle_{nl}$	$q_x^{(sp)}$	$q_y^{(sp)}$	$q_z^{(sp)}$
α	1s	-183.2759	0.0066	0.0000	0.0000	0.0000
α	2s	-21.4572	0.1250	0.0000	0.0000	0.0000
α	2p _x	-17.8273	0.1034	+0.0827	-0.0414	-0.0414
α	2p _y	-17.8273	0.1034	-0.0414	+0.0827	-0.0414
α	2p _z	-17.8244	0.1036	-0.0414	-0.0414	+0.0829
α	3s	-2.9463	1.1792	-0.0016	-0.0016	+0.0032
α	3p _z	-1.9071	1.4095	-0.5638	-0.5638	+1.1276
α	3p _x	-1.8680	1.4017	+1.1213	-0.5607	-0.5607
α	3p _y	-1.8680	1.4017	-0.5607	+1.1213	-0.5607
α	3d _{yz}	-0.4248	2.8534	-1.6305	+0.8153	+0.8153
α	3d _{zx}	-0.4248	2.8534	+0.8153	-1.6305	+0.8153
α	4s	-0.2338	15.4686	+0.0616	+0.0616	-0.1232
β	1s	-183.2754	0.0066	0.0000	0.0000	0.0000
β	2s	-21.4247	0.1247	+0.0001	+0.0001	-0.0001
β	2p _x	-17.8015	0.1031	+0.0825	-0.0412	-0.0412
β	2p _y	-17.8015	0.1031	-0.0412	+0.0825	-0.0412
β	2p _z	-17.7791	0.1030	-0.0412	-0.0412	+0.0824
β	3s	-2.8211	1.1778	+0.0172	+0.0172	-0.0344
β	3p _x	-1.7472	1.4036	+1.1229	-0.5614	-0.5614
β	3p _y	-1.7472	1.4036	-0.5614	+1.1229	-0.5614
β	3p _z	-1.6867	1.4105	-0.5642	-0.5642	+1.1284
β	4s	-0.2112	17.3797	+0.5815	+0.5815	-1.1629
Total			50.2249	-0.1625	-0.1625	+0.3249

Table C9 Same as Table C6, but for the Ni atom.

Spin	Orbital	ε_j	$\langle r^2 \rangle_{nl}$	$q_x^{(sp)}$	$q_y^{(sp)}$	$q_z^{(sp)}$
α	1s	-305.4079	0.0040	0.0000	0.0000	0.0000
α	2s	-37.7247	0.0720	0.0000	0.0000	-0.0001
α	2p _x	-32.7657	0.0574	+0.0459	-0.0230	-0.0230
α	2p _y	-32.7657	0.0574	-0.0230	+0.0459	-0.0230
α	2p _z	-32.7281	0.0574	-0.0229	-0.0229	+0.0459
α	3s	-4.7265	0.6527	+0.0073	+0.0073	-0.0147
α	3p _x	-3.1649	0.7371	+0.5897	-0.2948	-0.2948
α	3p _y	-3.1649	0.7371	-0.2948	+0.5897	-0.2948
α	3p _z	-3.0843	0.7415	-0.2966	-0.2966	+0.5932
α	3d _{x²-y²}	-0.5446	1.4257	+0.4073	+0.4073	-0.8147
α	3d _{xy}	-0.4962	1.5120	+0.4320	+0.4320	-0.8640
α	3d _{yz}	-0.4616	1.5739	-0.8994	+0.4497	+0.4497
α	3d _{zx}	-0.4616	1.5739	+0.4497	-0.8994	+0.4497
α	3d _{z²}	-0.4493	1.5996	-0.4427	-0.4427	+0.8854
α	4s	-0.2395	13.2134	+0.1360	+0.1360	-0.2720
β	1s	-305.4054	0.0040	0.0000	0.0000	0.0000
β	2s	-37.6883	0.0719	0.0000	0.0000	0.0000
β	2p _x	-32.7198	0.0572	+0.0458	-0.0229	-0.0229
β	2p _y	-32.7198	0.0572	-0.0229	+0.0458	-0.0229
β	2p _z	-32.7194	0.0573	-0.0229	-0.0229	+0.0459
β	3s	-4.6262	0.6549	-0.0005	-0.0005	+0.0010
β	3p _z	-3.0570	0.7407	-0.2963	-0.2963	+0.5926
β	3p _x	-3.0065	0.7383	+0.5907	-0.2953	-0.2953
β	3p _y	-3.0065	0.7383	-0.2953	+0.5907	-0.2953
β	3d _{xy}	-0.4702	1.4877	+0.4251	+0.4251	-0.8501
β	3d _{yz}	-0.4160	1.5895	-0.9083	+0.4541	+0.4541
β	3d _{zx}	-0.4160	1.5895	+0.4541	-0.9083	+0.4541
β	3d _{z²}	-0.3977	1.6301	-0.4655	-0.4655	+0.9309
Total			33.4318	-0.4074	-0.4074	+0.8148

Table C10 Same as Table C6, but for the Ga atom.

Spin	Orbital	ε_j	$\langle r^2 \rangle_{nl}$	$q_x^{(sp)}$	$q_y^{(sp)}$	$q_z^{(sp)}$
α	1s	-378.6802	0.0033	0.0000	0.0000	0.0000
α	2s	-47.5198	0.0623	0.0000	0.0000	0.0000
α	2p _z	-42.4832	0.0452	-0.0181	-0.0181	+0.0362
α	2p _x	-42.4826	0.0452	+0.0362	-0.0181	-0.0181
α	2p _y	-42.4826	0.0452	-0.0181	+0.0362	-0.0181
α	3s	-6.2558	0.5350	+0.0004	+0.0004	-0.0008
α	3p _x	-4.4690	0.5485	+0.4388	-0.2194	-0.2194
α	3p _y	-4.4690	0.5485	-0.2194	+0.4388	-0.2194
α	3p _z	-4.4678	0.5474	-0.2189	-0.2189	+0.4379
α	3d _{x²-y²}	-1.1813	0.7753	+0.2215	+0.2215	-0.4430
α	3d _{xy}	-1.1813	0.7753	+0.2215	+0.2215	-0.4430
α	3d _{yz}	-1.1761	0.7753	-0.4430	+0.2215	+0.2215
α	3d _{zx}	-1.1761	0.7753	+0.2215	-0.4430	+0.2215
α	3d _{z²}	-1.1743	0.7757	-0.2239	-0.2239	+0.4478
α	4s	-0.4471	7.5754	+0.0036	+0.0036	-0.0072
α	4p _z	-0.2086	13.9574	-5.5830	-5.5830	+11.1659
β	1s	-378.6792	0.0033	0.0000	0.0000	0.0000
β	2s	-47.5192	0.0623	0.0000	0.0000	0.0000
β	2p _x	-42.4823	0.0452	+0.0362	-0.0181	-0.0181
β	2p _y	-42.4823	0.0452	-0.0181	+0.0362	-0.0181
β	2p _z	-42.4796	0.0452	-0.0181	-0.0181	+0.0362
β	3s	-6.2535	0.5349	+0.0007	+0.0007	-0.0013
β	3p _x	-4.4682	0.5483	+0.4386	-0.2193	-0.2193
β	3p _y	-4.4682	0.5483	-0.2193	+0.4386	-0.2193
β	3p _z	-4.4585	0.5477	-0.2191	-0.2191	+0.4382
β	3d _{x²-y²}	-1.1808	0.7753	+0.2215	+0.2215	-0.4430
β	3d _{xy}	-1.1808	0.7753	+0.2215	+0.2215	-0.4430
β	3d _{yz}	-1.1720	0.7753	-0.4430	+0.2215	+0.2215
β	3d _{zx}	-1.1720	0.7753	+0.2215	-0.4430	+0.2215
β	3d _{z²}	-1.1691	0.7756	-0.2133	-0.2133	+0.4267
β	4s	-0.3877	7.3770	-0.0070	-0.0070	+0.0139
Total			41.4245	-5.5788	-5.5788	+11.1576

References

- [1] J. A. Maruhn, P.-G. Reinhard, and E. Suraud, *Simple Models of Many-Fermion Systems*, (Springer-Verlag, Berlin Heidelberg, 2010).
- [2] K. Hagino and Y. Maeno, *Found. Chem.*, **22**, 267 (2020).
- [3] Y. Maeno, K. Hagino, and T. Ishiguro, Three related topics on the periodic tables of elements, in press ().
- [4] Aage Bohr and Ben R. Mottelson, *Nuclear Deformations*, volume 2 of *Nuclear Structure*, (W. A. Benjamin, 1975).
- [5] P. Ring and P. Schuck, *The Nuclear Many-Body Problem*, (Springer-Verlag, Berlin Heidelberg, 1980).
- [6] J. Dobaczewski, W. Nazarewicz, J. Skalski, and T. Werner, *Phys. Rev. Lett.*, **60**, 2254 (1988).
- [7] A. Arima and H. Horie, *Prog. Theor. Phys.*, **11**, 509 (1954).
- [8] T. Minamisono, S. Fukuda, T. Ohtsubo, A. Kitagawa, Y. Nakayama, Y. Someda, S. Takeda, M. Fukuda, K. Matsuta, and Y. Nojiri, *Nucl. Phys. A*, **559**, 239 (1993).
- [9] T. Minamisono, K. Matsuta, K. Minamisono, S. Kudo, M. Ogura, S. Fukuda, K. Sato, M. Mihara, and M. Fukuda, *Hyperfine Interact.*, **136**, 225 (2001).
- [10] T. Ohtsubo, N. J. Stone, J. R. Stone, I. S. Towner, C. R. Bingham, C. Gaulard, U. Köster, S. Muto, J. Nikolov, K. Nishimura, G. S. Simpson, G. Soti, M. Veskovcic, W. B. Walters, and F. Wauters, *Phys Rev Lett*, **109**, 032504 (2012).
- [11] H. Sagawa and B. Alex Brown, *Nucl. Phys. A*, **430**, 84 (1984).
- [12] H. Morinaga, *Phys. Rev.*, **101**, 254 (1956).
- [13] H. Morinaga, *Phys. Lett.*, **21**, 78 (1966).
- [14] K. Ikeda, N. Takigawa, and H. Horiuchi, *Prog. Theor. Phys. Suppl.*, **E68**, 464 (1968).
- [15] Y. Kanada-En'yo, H. Horiuchi, and A. Doté, *Phys. Rev. C*, **60**, 064304 (1999).
- [16] N. Itagaki, S. Okabe, K. Ikeda, and I. Tanihata, *Phys. Rev. C*, **64**, 014301 (2001).
- [17] W. von Oertzen, M. Freer, and Y. Kanada-En'yo, *Phys. Rep.*, **432**, 43 (2006).
- [18] M. Itoh, H. Akimune, M. Fujiwara, U. Garg, N. Hashimoto, T. Kawabata, K. Kawase, S. Kishi, T. Murakami, K. Nakanishi, Y. Nakatsugawa, B. K. Nayak, S. Okumura, H. Sakaguchi, H. Takeda, S. Terashima, M. Uchida, Y. Yasuda, M. Yosoi, and J. Zenihiro, *Phys. Rev. C*, **84**, 054308 (2011).
- [19] M. Freer and H.O.U. Fynbo, *Prog. Part. Nucl. Phys.*, **78**, 1 (2014).
- [20] T. Baba and M. Kimura, *Phys. Rev. C*, **94**, 044303 (2016).
- [21] T. Baba and M. Kimura, *Phys. Rev. C*, **95**, 064318 (2017).
- [22] N. Itagaki and T. Naito, Consistent description for cluster dynamics and single-particle correlation (2020), arXiv:2011.12642.
- [23] R. C. Johnson and R. R. Rettew, *J. Chem. Educ.*, **42**, 145 (1965).
- [24] I. Cohen, *J. Chem. Educ.*, **42**, 397 (1965).
- [25] H. Friedrich, *Theoretical Atomic Physics*, (Springer-Verlag, Berlin Heidelberg, 2006).
- [26] H. A. Fertig and W. Kohn, *Phys. Rev. A*, **62**, 052511 (2000).
- [27] A. Borgoo, O. Scharf, G. Gaigalas, and M. Godefroid, *Comput. Phys. Commun.*, **181**, 426 (2010).
- [28] B. J. Austin, V. Heine, and L. J. Sham, *Phys. Rev.*, **127**, 276 (1962).
- [29] S. G. Louie, S. Froyen, and M. L. Cohen, *Phys. Rev. B*, **26**, 1738 (1982).
- [30] R. M. Martin, *Electronic Structure*, (Cambridge University Press, Cambridge, 2004).
- [31] P. Schwerdtfeger, *ChemPhysChem*, **12**, 3143 (2011).
- [32] C. C. J. Roothaan, *Rev. Mod. Phys.*, **23**, 69 (1951).
- [33] J. A. Pople and R. K. Nesbet, *J. Chem. Phys.*, **22**, 571 (1954).
- [34] G. Berthier, *C. R. Acad. Sci.*, **238**, 91 (1954).
- [35] R. McWeeny and G. Diercksen, *J. Chem. Phys.*, **49**, 4852 (1968).
- [36] F. Jensen, *Introduction to Computational Chemistry*, (John Wiley & Sons, Chichester, third edition, 2017).
- [37] Chr. Møller and M. S. Plesset, *Phys. Rev.*, **46**, 618 (1934).
- [38] F. Coester, *Nucl. Phys.*, **7**, 421 (1958).
- [39] J. Čížek, *J. Chem. Phys.*, **45**, 4256 (1966).
- [40] J. Čížek and J. Paldus, *Int. J. Quantum Chem.*, **5**, 359 (1971).
- [41] J. A. Pople, J. S. Binkley, and R. Seeger, *Int. J. Quantum Chem.*, **10**, 1 (1976).
- [42] J. A. Pople, R. Seeger, and R. Krishnan, *Int. J. Quantum Chem.*, **12**, 149 (1977).
- [43] K. Raghavachari and J. A. Pople, *Int. J. Quantum Chem.*, **14**, 91 (1978).
- [44] R. Krishnan, H. B. Schlegel, and J. A. Pople, *J. Chem. Phys.*, **72**, 4654 (1980).
- [45] G. W. Trucks, E.A. Salter, C. Sosa, and R. J. Bartlett, *Chem. Phys. Lett.*, **147**, 359 (1988).
- [46] M. Head-Gordon, John A. Pople, and M. J. Frisch, *Chem. Phys. Lett.*, **153**, 503 (1988).
- [47] K. Raghavachari, J. A. Pople, E. S. Replogle, and M. Head-Gordon, *J. Phys. Chem.*, **94**, 5579 (1990).

-
- [48] J. A. Pople, *Rev. Mod. Phys.*, **71**, 1267 (1999).
- [49] P. Hohenberg and W. Kohn, *Phys. Rev.*, **136**, B864 (1964).
- [50] W. Kohn and L. J. Sham, *Phys. Rev.*, **140**, A1133 (1965).
- [51] W. Kohn, *Rev. Mod. Phys.*, **71**, 1253 (1999).
- [52] S. G. Nilsson, *Dan. Mat. Fys. Medd.*, **29**, 1 (1955).
- [53] B. R. Mottelson and S. G. Nilsson, *Phys. Rev.*, **99**, 1615 (1955).
- [54] I. Ragnarsson and S. G. Nilsson, *Shapes and Shells in Nuclear Structure*, (Cambridge University Press, Cambridge, 2005).
- [55] M. A. Blanco, M. Flórez, and M. Bermejo, *J. Mol. Struct.*, **419**, 19 (1997).
- [56] M. J. Frisch, G. W. Trucks, H. B. Schlegel, G. E. Scuseria, M. A. Robb, J. R. Cheeseman, G. Scalmani, V. Barone, G. A. Petersson, H. Nakatsuji, X. Li, M. Caricato, A. V. Marenich, J. Bloino, B. G. Janesko, R. Gomperts, B. Mennucci, H. P. Hratchian, J. V. Ortiz, A. F. Izmaylov, J. L. Sonnenberg, D. Williams-Young, F. Ding, F. Lipparini, F. Egidi, J. Goings, B. Peng, A. Petrone, T. Henderson, D. Ranasinghe, V. G. Zakrzewski, J. Gao, N. Rega, G. Zheng, W. Liang, M. Hada, M. Ehara, K. Toyota, R. Fukuda, J. Hasegawa, M. Ishida, T. Nakajima, Y. Honda, O. Kitao, H. Nakai, T. Vreven, K. Throssell, J. A. Montgomery, Jr., J. E. Peralta, F. Ogliaro, M. J. Bearpark, J. J. Heyd, E. N. Brothers, K. N. Kudin, V. N. Staroverov, T. A. Keith, R. Kobayashi, J. Normand, K. Raghavachari, A. P. Rendell, J. C. Burant, S. S. Iyengar, J. Tomasi, M. Cossi, J. M. Millam, M. Klene, C. Adamo, R. Cammi, J. W. Ochterski, R. L. Martin, K. Morokuma, O. Farkas, J. B. Foresman, and D. J. Fox, *Gaussian 16 Revision A.03* (2016), Gaussian Inc. Wallingford CT.
- [57] P. J. Mohr, D. B. Newell, and B. N. Taylor, *Rev. Mod. Phys.*, **88**, 035009 (2016).
- [58] E. Tiesinga, P. J. Mohr, D. B. Newell, and B. N. Taylor, *The 2018 CODATA Recommended Values of the Fundamental Physical Constants* (2019).
- [59] J. P. Perdew and Alex Zunger, *Phys. Rev. B*, **23**, 5048 (1981).
- [60] W. J. Hehre, R. Ditchfield, and J. A. Pople, *J. Chem. Phys.*, **56**, 2257 (1972).
- [61] T. Clark, J. Chandrasekhar, G. W. Spitznagel, and P. Von Ragué Schleyer, *J. Comput. Chem.*, **4**, 294 (1983).
- [62] D. E. Woon and T. H. Dunning, *J. Chem. Phys.*, **98**, 1358 (1993).
- [63] K. A. Peterson, D. E. Woon, and T. H. Dunning, *J. Chem. Phys.*, **100**, 7410 (1994).
- [64] W. J. Hehre, R. F. Stewart, and J. A. Pople, *J. Chem. Phys.*, **51**, 2657 (1969).
- [65] A. Kramida, Yu. Ralchenko, J. Reader, and NIST ASD Team, *NIST Atomic Spectra Database* (ver. 5.7.1), [Online]. Available: <https://physics.nist.gov/asd> [2020, July 30]. National Institute of Standards and Technology, Gaithersburg, MD. (2019).
- [66] J. P. Foster and F. Weinhold, *J. Am. Chem. Soc.*, **102**, 7211 (1980).
- [67] J. E. Carpenter and F. Weinhold, *J. Mol. Struct.*, **169**, 41 (1988).
- [68] A. E. Reed, L. A. Curtiss, and F. Weinhold, *Chem. Rev.*, **88**, 899 (1988).
- [69] E. D. Glendenning, A. E. Reed, J. E. Carpenter, and F. Weinhold, *NBO Version 3.1* (), Gaussian Inc. Wallingford CT.
- [70] F. A. Cotton, G. Wilkinson, and P. L. Gaus, *Basic Inorganic Chemistry*, (John Wiley & Sons, Chichester, 1995).
- [71] F. Hund, *Z. Phys.*, **34**, 296 (1925).
- [72] F. Hund, *Z. Phys.*, **33**, 345 (1925).
- [73] J. C. Slater, *Phys. Rev.*, **34**, 1293 (1929).
- [74] K. Hongo, R. Maezono, Y. Kawazoe, H. Yasuhara, M. D. Towler, and R. J. Needs, *J. Chem. Phys.*, **121**, 7144 (2004).
- [75] T. Oyamada, K. Hongo, Y. Kawazoe, and H. Yasuhara, *J. Chem. Phys.*, **133**, 164113 (2010).
- [76] L. Schiff, *Quantum Mechanics*, (McGraw-Hill, New York, third edition, 1968).
- [77] R. G. Parr, Density functional theory of atoms and molecules, In *Horizons of quantum chemistry*, page 5. Springer, Dordrecht (1980).
- [78] B. D. Serot and J. D. Walecka, The Relativistic Nuclear Many-Body Problem, In J.W. Negele and E. Vogt, editors, *Advances in Nuclear Physics*, volume 16. Plenum Press (1986).
- [79] O. Bohigas, A.M. Lane, and J. Martorell, *Phys. Rep.*, **51**, 267 (1979).
- [80] G. F. Bertsch and H. Feldmeier, *Phys. Rev. C*, **56**, 839 (1997).
- [81] H. Yukawa, *Proc. Phys. Math. Soc. Jpn. Third*, **17**, 48 (1935).
- [82] V. G. J. Stoks, R. A. M. Klomp, C. P. F. Terheggen, and J. J. de Swart, *Phys. Rev. C*, **49**, 2950 (1994).
- [83] R. B. Wiringa, V. G. J. Stoks, and R. Schiavilla, *Phys. Rev. C*, **51**, 38 (1995).
- [84] R. Machleidt, *Phys. Rev. C*, **63**, 024001 (2001).
- [85] N. Ishii, S. Aoki, and T. Hatsuda, *Phys. Rev. Lett.*, **99**, 022001 (2007).
- [86] K. S. Krane, *Introductory Nuclear Physics*, (John Wiley & Sons, Chichester, 1988).
- [87] B. Povh, K. Rith, C. Scholz, and F. Zetsche, *Particles and Nuclei*, (Springer-Verlag, Berlin Heidelberg,

- 2008).
- [88] M. Bender, P.-H. Heenen, and P.-G. Reinhard, *Rev. Mod. Phys.*, **75**, 121 (2003).
 - [89] N. Bohr and J. A. Wheeler, *Phys. Rev.*, **56**, 426 (1939).
 - [90] B. Povh, K. Rith, C. Scholz, F. Zetsche, and W. Rodejohann, *Particles and Nuclei*, (Springer-Verlag, Berlin Heidelberg, 2015).
 - [91] E. Engel and R. M. Dreizler, *Density Functional Theory—An Advanced Course*, Theoretical and Mathematical Physics. (Springer-Verlag, Berlin, Heidelberg, 2011).
 - [92] E. Wigner, *Phys. Rev.*, **46**, 1002 (1934).
 - [93] D. Vautherin and D. M. Brink, *Phys. Rev. C*, **5**, 626 (1972).
 - [94] D. Vautherin, *Phys. Rev. C*, **7**, 296 (1973).
 - [95] T. F. Gallagher, *Rydberg atoms*, volume 3, (Cambridge University Press, Cambridge, 2005).
 - [96] M. Saffman, T. G. Walker, and K. Mølmer, *Rev. Mod. Phys.*, **82**, 2313 (2010).
 - [97] P. J. J. Luukko and J.-M. Rost, *Phys. Rev. Lett.*, **119**, 203001 (2017).
 - [98] A. S. Stodolna, A. Rouzée, F. Lépine, S. Cohen, F. Robicheaux, A. Gijsbertsen, J. H. Jungmann, C. Bordas, and M. J. J. Vrakking, *Phys. Rev. Lett.*, **110**, 213001 (2013).
 - [99] S. Cohen, M. M. Harb, A. Ollagnier, F. Robicheaux, M. J. J. Vrakking, T. Barillot, F. Lépine, and C. Bordas, *Phys. Rev. A*, **94**, 013414 (2016).
 - [100] J. Itatani, J. Levesque, D. Zeidler, H. Niikura, H. Pépin, J. C. Kieffer, P. B. Corkum, and D. M. Villeneuve, *Nature*, **432**, 867 (2004).
 - [101] B. S. Pudliner, A. Smerzi, J. Carlson, V. R. Pandharipande, Steven C. Pieper, and D. G. Ravenhall, *Phys. Rev. Lett.*, **76**, 2416 (1996).
 - [102] A. Smerzi, D. G. Ravenhall, and V. R. Pandharipande, *Phys. Rev. C*, **56**, 2549 (1997).
 - [103] S. Gandolfi, J. Carlson, and Steven C. Pieper, *Phys. Rev. Lett.*, **106**, 012501 (2011).
 - [104] S. K. Bogner, R. J. Furnstahl, H. Hergert, M. Kortelainen, P. Maris, M. Stoitsov, and J. P. Vary, *Phys. Rev. C*, **84**, 044306 (2011).
 - [105] P. Maris, J. P. Vary, S. Gandolfi, J. Carlson, and S. C. Pieper, *Phys. Rev. C*, **87**, 054318 (2013).
 - [106] S. Shen, H. Liang, J. Meng, P. Ring, and S. Zhang, *Phys. Rev. C*, **97**, 054312 (2018).
 - [107] S. Shen, G. Colò, and X. Roca-Maza, *Phys. Rev. C*, **99**, 034322 (2019).
 - [108] Z. Wang, T. Naito, H. Liang, and W. H. Long, Exploring effects of tensor force and its strength via neutron drops (2021), arXiv:2101.04860.
 - [109] P. W. Zhao and S. Gandolfi, *Phys. Rev. C*, **94**, 041302 (2016).
 - [110] P A Zyla, R M Barnett, J Beringer, O Dahl, D A Dwyer, D E Groom, C J Lin, K S Lugovsky, E Pianori, D J Robinson, C G Wohl, W M Yao, K Agashe, G Aielli, B C Allanach, C Amsler, M Antonelli, E C Aschenauer, D M Asner, H Baer, Sw Banerjee, L Baudis, C W Bauer, J J Beatty, V I Belousov, S Bethke, A Bettini, O Biebel, K M Black, E Blucher, O Buchmuller, V Burkert, M A Bychkov, R N Cahn, M Carena, A Ceccucci, A Cerri, D Chakraborty, R Sekhar Chivukula, G Cowan, G D’Ambrosio, T Damour, D de Florian, A de Gouvêa, T DeGrand, P de Jong, G Dissertori, B A Dobrescu, M D’Onofrio, M Doser, M Drees, H K Dreiner, P Eerola, U Egede, S Eidelman, J Ellis, J Erler, V V Ezhela, W Fetscher, B D Fields, B Foster, A Freitas, H Gallagher, L Garren, H J Gerber, G Gerbier, T Gershon, Y Gershtein, T Gherghetta, A A Godizov, M C Gonzalez-Garcia, M Goodman, C Grab, A V Gritsan, C Grojean, M Grünewald, A Gurtu, T Gutsche, H E Haber, C Hanhart, S Hashimoto, Y Hayato, A Hebecker, S Heinemeyer, B Heltsley, J J Hernández-Rey, K Hikasa, J Hisano, A Höcker, J Holder, A Holtkamp, J Huston, T Hyodo, K F Johnson, M Kado, M Karliner, U F Katz, M Kenzie, V A Khoze, S R Klein, E Klempt, R V Kowalewski, F Krauss, M Kreps, B Krusche, Y Kwon, O Lahav, J Laiho, L P Lellouch, J Lesgourgues, A R Liddle, Z Ligeti, C Lippmann, T M Liss, L Littenberg, C Lourenço, S B Lugovsky, A Lusiani, Y Makida, F Maltoni, T Mannel, A V Manohar, W J Marciano, A Masoni, J Matthews, U G Meißner, M Mikhasenko, D J Miller, D Milstead, R E Mitchell, K Mönig, P Molaro, F Moortgat, M Moskvic, K Nakamura, M Narain, P Nason, S Navas, M Neubert, P Nevski, Y Nir, K A Olive, C Patrignani, J A Peacock, S T Petcov, V A Petrov, A Pich, A Piepke, A Pomarol, S Profumo, A Quadt, K Rabbertz, J Rademacker, G Raffelt, H Ramani, M Ramsey-Musolf, B N Ratcliff, P Richardson, A Ringwald, S Roesler, S Rolli, A Romaniouk, L J Rosenberg, J L Rosner, G Rybka, M Ryskin, R A Ryutin, Y Sakai, G P Salam, S Sarkar, F Sauli, O Schneider, K Scholberg, A J Schwartz, J Schwiening, D Scott, V Sharma, S R Sharpe, T Shutt, M Silari, T Sjöstrand, P Skands, T Skwarnicki, G F Smoot, A Soffer, M S Sozzi, S Spanier, C Spiering, A Stahl, S L Stone, Y Sumino, T Sumiyoshi, M J Syphers, F Takahashi, M Tanabashi, J Tanaka, M Taševský, K Terashi, J Terning, U Thoma, R S Thorne, L Tiator, M Titov, N P Tkachenko, D R Tovey, K Trabelsi, P Urquijo, G Valencia, R Van de Water, N Varelas, G Venanzoni, L Verde, M G Vinciter, P Vogel, W Vogelsang, A Vogt, V Vorobyev, S P Wakely, W Walkowiak, C W Walter, D Wands, M O Wascko, D H Weinberg, E J Weinberg, M White, L R Wiencke, S Willocq, C L Woody, R L Workman, M Yokoyama, R Yoshida, G Zanderighi, G P Zeller, O V Zenin, R Y Zhu, S L Zhu, F Zimmermann, J Anderson, T Basaglia, V S Lugovsky, P Schaffner, and W Zheng, *Prog.*

-
- Theor. Exp. Phys., **2020**(8), 083C01 (08 2020).
- [111] J. Bartel, P. Quentin, M. Brack, C. Guet, and H.-B. Håkansson, Nucl. Phys. A, **386**, 79 (1982).